Spatial Temperature and Concentration Changes Following Heterogeneous Damage To a Model Diesel Oxidation Catalyst

by

April Elizabeth Russell

A thesis

presented to the University of Waterloo

in fulfilment of the

thesis requirement for the degree of

Master of Applied Science

in

Chemical Engineering

Waterloo, Ontario, Canada, 2010

AUTHOR'S DECLARATION

I hereby declare that I am the sole author of this thesis. This is a true copy of the thesis, including any require final revisions, as accepted by my examiners.

I understand that my thesis may be made electronically available to the public.

Abstract

Infra-Red thermography and spatially-resolved capillary inlet mass spectrometry (SpaciMS) have been used to characterize propylene oxidation along a Pt/Al_2O_3 monolith-supported catalyst, before and after heterogeneous deactivation. The combined techniques clearly show reaction location, and therefore catalyst use, and how these change with thermal and sulphur degradation.

Following the heterogeneous thermal aging, the reaction zones at steady state were broader and located farther into the catalyst relative to those observed with the fresh catalyst. As well, the time for the temperature and concentration waves to travel through the catalyst during back-to-front ignition increased. These effects were more pronounced with 1500 ppm propylene relative to 4500 ppm propylene. Such trends could not be detected based on standard catalyst-outlet measurements. The light-off behaviour was also impacted by the aging, resulting in complex changes to the temperature front propagation, depending on the propylene concentration.

With each sulphur exposure step, light-off temperatures increased and the time for back-to-front ignition during temperature programmed oxidation changed pattern. With 1500 ppm propylene fed, the reaction zones established during steady-state operation shifted farther into the catalyst and increased slightly in width following sulphur treatment; at very high temperature and for 4500 ppm propylene, the reaction zones were very close to the catalyst inlet and virtually indistinguishable between catalyst sulphation states. However, at lower steady-state temperatures for the higher propylene concentration, the catalyst did experience delays in reaction light-off and light-off position moved downstream in the catalyst with sulphur damage.

Acknowledgements

I would like to thank my supervisor Professor William Epling for his encouragement, guidance, and support during my study. I am also thankful for the help of my colleagues through all the difficulties I encountered. Furthermore, the support of my family and friends was essential to the successful completion of this work.

I would also like to express my appreciation to Professor William Anderson and Professor Yuning Li for their time and helpful comments in reviewing this thesis.

I would like to thank the Natural Sciences and Engineering Research Council of Canada (NSERC) Discovery Grant Program and Cummins for their financial support.

Table of Contents

List of Figures

List of Tables

Chapter 1. Introduction

Some of the data contained in this thesis, and its analysis, have been previously published by Russell et al, Ind. Eng. Chem. Res. DOI: 10.1021/ie1005299.

1.1 Research Aim

The aim of this research is to compare reaction pattern changes on a diesel oxidation catalyst that occur following heterogeneous catalyst degradation processes. The specific goals of this project are:

1. Investigate the spatial reaction pattern changes following heterogeneous thermal degradation
2. Investigate the spatial reaction pattern changes following heterogeneous sulphur degradation.

1.2 Automobile Emissions

Compared to the current standard gasoline engine, which burns fuel and oxygen (from the air) in stoichiometric proportion, lean-burn (excess oxygen) engines are inherently more fuel efficient[1,2], a property that has become more important lately due to concerns over environmental impacts and fuel reserves. As such, some groups have proposed CO_2 emission targets[3], a move that will likely result in wider diesel engine use because of their greater fuel efficiency allows the lower CO_2 production. Already there are indications that diesel engines are becoming more common in the passenger vehicle market[2,4].

Incomplete combustion in diesel engines creates CO and unburned hydrocarbons, and soot or particulate matter (PM)[5]. Hydrocarbon reactions can form polynuclear aromatic components and other volatile organic carbon compounds, which can themselves be emissions or further react to NO_X in sunlight[5]. NO and NO_2, collectively called NO_X, form from the nitrogen in air during combustion, and to a very minor extent from fuel-bound nitrogen[5]. While NO_X emissions are themselves pollutants, they also undergo photochemical reactions to generate ozone, which is a strong oxidizer, irritant, and smog component[5,6]. In general, the cooler engine temperatures for diesels, compared to gasoline engines, generate less NO_X at the expense of higher PM emissions[7]. Until recently PM emissions were of greater importance in the emissions regulations and therefore many engine and exhaust treatment modifications were focussed on lowering PM at the expense of higher NO_X. Control of these two components is more difficult at lower diesel exhaust catalyst temperatures, between 200-300°C for light-duty engines or 300-450°C for heavy-duty engines[5], with changes to decrease the production of one often causing an increase in production for the other.

Treatment of diesel exhaust is more difficult than gasoline exhaust since the former contains gaseous, liquid, and solid components[4,8]. These differences in exhaust conditions are caused by the engine design differences, where a diesel engine injects only the required amount fuel into compressed hot air to generate the desired power resulting in a fuel-lean environment[5].

The detrimental environmental and health effects of emissions from fossil fuel internal combustion engines have led governments in developed countries to regulate emissions

from vehicles[4,9,10]. These regulations, particularly those of the USA[11] and Europe[12], have become increasingly stringent since their introduction in the 1970s.

CO and hydrocarbon emissions were the first to be regulated[13]. Initially engine modifications were used to alter the emissions production, but over time engine aftertreatment systems , more specifically post-engine catalysts, were required to meet the emissions limits of the 1970 Clean Air Act[11]. Transition metals, such as copper and nickel, and other base metals were deemed too sensitive to fuel contaminants and lacked sufficient thermal durability for automotive use[14]. Platinum group metals, including platinum (Pt), palladium (Pd), and rhodium (Rh), showed good oxidation performance along with good thermal durability, and as such have been used in catalytic converters since the beginning[13]. Rh is used primarily for NO_X reduction and is included in the three-way catalyst (TWC) for gasoline engines[13]. Diesel oxidation catalysts (DOCs) with Pt and/or Pd provide high oxidation activity for CO, unburned hydrocarbons, and liquid hydrocarbons (soluble organic fraction (SOF) components).[4] Oxidation of SOF is beneficial since it can reduce PM emissions[2]. Pt and Pd can also provide NO oxidation activity, which can be exploited to improve the performance of downstream NO_X abatement systems[15] and some soot filters[13,16]. Unfortunately, these precious metal catalysts also catalyze the oxidation of SO_2. Finding an appropriately selective oxidation catalyst has been difficult.

In stoichiometric-burn gasoline engines, three-way catalysts (TWC) readily reduce NO_X to N_2 using CO and hydrocarbons in the absence of excess oxygen. However, the higher air-to-fuel ratio (fuel-lean, oxygen-rich environment) of diesel engine exhaust

makes reduction of NO_X species more difficult. In order to remove NO_X from the diesel exhaust, NO_X abatement systems, such as the lean NO_X trap (LNT) or NO_X storage and reduction (NSR)[17-20] and selective catalytic reduction (SCR)[21, 22], are placed downstream of DOCs in the exhaust train[1]. This arrangement uses the NO oxidation capacity of the DOC to provide NO_2 to the NO_X abatement catalysts. A mixture of NO and NO_2 can provide better NO_X removal performance than NO alone[5,13,17,23-29], especially at operating temperatures below 250°C[22]. However, NO is the primary constituent of NO_X in diesel exhaust[27,30,31], approximately 90%[5]; thus, the DOC provides a primary function for CO and hydrocarbon oxidation and an additional secondary function of NO oxidation for improved NO_X removal.

Particulate matter (PM), also called soot, is the solid component of diesel exhaust that contributes to smog and respiratory distress. Black soot forms when small droplets of fuel leave a core of carbon particles that adsorb hydrocarbons, sulphur, NO_X, and water. Physical changes to engines and combustion control improvements have reduced the amount of PM produced, although complete elimination has not been achieved[13]. While the upstream DOC provides some SOF oxidation at low temperatures to reduce the potential soot load, a diesel particulate filter (DPF) is required to capture the bulk of the PM produced. Current DPFs use catalytic components on a wall-flow filter, or catalyzed-DPF (cDPF), where exhaust enters channels that are blocked at the filter outlet, forcing the gas through the filter wall where the alternating filter inlet ends are blocked[13]. For passenger vehicles and other applications where exhaust temperatures are lower (low speed), the DPF requires periodic regeneration at elevated temperatures to achieve soot oxidation. These temperature excursions are achieved by fuel injection into the exhaust that is oxidized over the DOC catalyst to generate a large exotherm.

The necessary exhaust temperature range to oxidize soot for an uncatalyzed DPF is 600-700°C, while a catalyzed DPF might require temperatures of only 350-450°C[5]. The Continuously Regenerating Trap[13,16] is a type of soot filter that uses NO_2 to oxidize soot from the filter continuously and at much lower temperatures (300°C)[32] than with oxygen alone (500-600°C)[1,16,33]. However, this system requires higher temperatures for NO oxidation in the upstream DOC, and so is restricted to use in heavy-duty diesels (buses, trucks, etc.) that can achieve these temperatures. The presence of sulphur oxides in the exhaust contributes to the amount of soot produced (i.e. increased PM emissions)[5]. While multiple components are required to achieve regulated emissions levels for diesel engines, the DOC plays an important role in the performance of each component and the overall emission reduction.

1.3 Exhaust System Configuration Effects

Component configuration has been studied to improve the performance of the diesel exhaust emission reduction systems. The location of the DOC in the exhaust train affects the temperatures of the catalyst, and thus the oxidation performance, with the longer the distance between the engine and catalyst lowering the temperature, and so delaying light-off of the oxidation reactions. Traditionally, the DOC is the first exhaust component after the engine and has often been located in the underfloor position. However, many systems have used a single catalyst near the engine (close-coupled) or two catalysts, with one very close to the engine as a pre-oxidation catalyst and another in the underfloor position[34]. The placement of catalysts must also consider expected catalyst damage and available space.

1.4 Emissions Abatement Shortcomings

Catalyst deactivation is a constant concern for catalytic converters because it is a natural phenomenon induced by several causes. The nature of automotive applications demands reliable performance over an extended time period with transient operating conditions. Efforts to reduce the amount of deactivation and mitigate the effects of the damage that does occur are very important. The study of deactivation is usually conducted with synthetic aging, which attempts to simulate the effects of vehicle aging in a shorter time frame and for less cost. Thermal aging (sintering) and sulphur poisoning (sulphation) are the two most common deactivation modes, and both types can be achieved in the laboratory with simulated aging.

Chapter 2. Literature Review

This chapter comprises a literature review of pertinent topics related to the research goals, including the diesel oxidation catalyst composition, hydrocarbon oxidation, catalyst thermal deactivation, catalyst sulphur degradation, and spatial reaction measurement techniques.

2.1 Diesel Oxidation Catalyst Composition

Diesel oxidation catalysts (DOCs) are commonly placed in diesel engine exhaust gas aftertreatment systems as discussed above, with targeted reactions including CO, hydrocarbon (HC), and NO oxidation. The first generation of catalytic converters used catalyst pellets in a packed bed, however their use in mobile applications led to unacceptably high rates of attrition. Instead, a ceramic monolith structure was introduced for its superior strength due to the low porosity of the ceramic that makes the monolith unsuitable to maintain a dispersed catalyst. To mitigate this effect, a high surface area material called the washcoat or catalyst support is adhered to the solid structure surface, and the catalytic metal is then dispersed on the washcoat[13]. Advances in manufacturing methods have allowed properties of the monolith to be optimized through alterations to the thermal stability of the active component and support, surface area, pore volume, and surface reactivity[35,36].

The washcoat or catalyst support material must have a high surface area to allow adhesion of the catalytic component. Alumina (Al_2O_3), silica (SiO_2), and zeolites, as well as combinations of these components, are common catalyst support materials, with

alumina the most common [37, 38,39]. The properties and preparation technique of different materials determine their use in different systems. For example, hydrothermal treatment of Al_2O_3 supports, provided by steam exposure at high temperatures (700-900°C), created Al_2O_3 with lower surface area and larger pore size compared to thermally treated catalysts[40,41]. Skoglundh[41] observed better light-off performance for CO and xylene with Al_2O_3 washcoats that were hydrothermally treated before the precious metal was deposited than that of supports that were only thermally treated. This occurs because a larger pore size provides less diffusion resistance for large molecules (xylene), while the impact of larger pores is less significant for the oxidation of the smaller CO molecule. The hydrothermally treated catalysts also had larger Pt particle size than those of the thermally treated supports, which may have an entwined effect on oxidation performance, as larger particles have higher specific activity than smaller particles[42]. Ishikawa[43] and Yoshida[44] examined the effect of the electric properties of the washcoat on Pt-oxide formation, and proposed that an acidic (i.e. electrophilic) support, such as Al_2O_3 and SiO_2, leads to a lower electron density on the Pt, especially compared to less acidic supports (lower acid strength, more positive pKa) such as ZrO_2 and La_2O_3, and as such these acidic washcoats mitigate Pt-oxide formation. Pt-oxides are undesired for oxidation reactions because the Pt-oxides block active surface sites for chemisorption.

The precious metal component is the reactive component. The most common precious metals used for DOCs are Pt and Pd[13,45], with increased use of Pd seen as a good method of lowering DOC costs by replacing expensive Pt. Traditionally, both Pd[5] and Rh[7] are more common as sole components in TWC or gasoline engine oxidation catalysts than in DOCs. Hydrocarbon oxidation occurs at lower temperatures over Pt compared to Pd and Rh when there is no CO in the feed gas[46]. Furthermore, Patterson

et al[46] concluded that these metals oxidized individual HC species in different orders, specifically the lowest light-off temperature occurred for benzene on Pt, toluene on Pd, and hexene on Rh, while in a HC mixture all metals show the same oxidation order of 1-hexene, toluene, followed by benzene. This effect is related to the relative adsorption strength of the reactants, including oxygen, on the metals. The adsorption strength is weaker when the electrons are more delocalized, such as those of the unsaturated HC, causing aromatics to adsorb less strongly than hexene, at least in the absence of water[46]. Additionally, the described effects are not additive or separate, making modeling more difficult.

A difficulty that can arise in catalyst design is that the bulk properties of components do not necessarily reflect the properties of these components in small, dispersed, and/or supported particle states, as the precious metals are[35]. A highly dispersed state is desired for the metal, as activity generally increases with the surface-to-bulk (higher surface area for reaction) ratio of the particles, although there is a lower limit on particle size[4]. Precious metal particle size depends on many factors including the preparation method (incipient wetness impregnation or wet impregnation), the support/washcoat[47], the precious metal precursor salt, and the pretreatment conditions (atmosphere, time, temperature, etc.)[48]. As well, activity can be affected by the surface structure of the active metal, an attribute referred to as structure sensitivity[49], which will be discussed in more detail in Section 2.2. This sensitivity relates to the type of surface sites exposed to the reaction atmosphere, with the relative amounts of these species changing with particle size. Each reaction can proceed at different rates over different metal sites.

Furthermore, the formation of Pt-oxides from exposure to O_2 or NO_2[26,27,50] decreases the oxidation performance of the catalyst for HC oxidation[51] and NO[26,27]. It was reported by Putna et al[52] that small particles appear to adsorb more oxygen due to structural differences[53] and that about three times the amount of oxygen on the metal at higher temperatures, indicating stronger interactions between oxygen and the small Pt particles (i.e. Pt-oxides).[52] Considering these different perspectives, there is likely an optimal Pt particle size for good oxidation performance that is more resistant to Pt-oxide formation.

2.2 Hydrocarbon Oxidation

Many different HCs exist in diesel exhaust, including aromatics, saturated, and unsaturated components. Generally, propylene is used as a model unsaturated HC and propane as a model saturated HC for the study of oxidation performance on catalysts[46]. Different HC and HC mixtures show different rates of reaction[46,54,55]. For example, alkanes tend to show slower reaction rates as the carbon chain length increases because more adjacent sites are required to achieve the adsorption of the HC chains[56]. Oxygen coverage on the metal itself is also important, as Luss et al[57] discussed the appearance of oscillations for propylene oxidation due to a process of Pt particle oxidation and reduction, with higher activity when the Pt is in the reduced (metallic) state. The oscillation phenomenon occurs because propylene and oxygen compete for active sites on the catalyst[58].

While both Pt and Pd adsorb oxygen and HC, Pt has a lower surface oxygen coverage[56] and is considered to have higher oxidation activity[36,56]. Pt also exhibits better performance for higher molecular weight HCs than Pd[59]. When extreme temperatures

are not required, Pt provides good oxidation activity and sufficient activity when SO_2 is present. However, at high temperatures, such as those generated in the DOC for DPF regeneration, the Pt activity declines due to thermal degradation[60].

Most kinetic studies for HC oxidation examine only one component at a time [61,62], and often at low concentrations. However, in practical applications, multiple HCs and other components are present in the exhaust. Co-inhibition of oxidation is common in multi-HC systems, and these effects will be discussed further below. Similarly, mixtures of CO and propylene have an inhibition effect on the conversion of the other component that diminishes as temperatures increase, while the inhibition of the oxidation by NO increases with temperature[58]. Conversely, HCs and CO also inhibit NO oxidation[1]. Irani et al[63] noted that NO_2 improved propylene conversion because NO_2 is a strong oxidant. However, oxidation of propylene by NO_2 regenerated the NO species. The HC oxidation performance effect diminished as temperatures, and thus NO concentration, increased[63].

Unsaturated HCs exhibit inverse-order (negative reaction order) dependencies on the oxidation rate[64], which follows a Langmuir-Hinselwood[61] dual-site[58,65] mechanism between adsorbed O_2 and HC, where the surface reaction between the two is rate limiting. At temperatures below light-off, HC adsorption is stronger than oxygen adsorption, limiting surface oxygen for reaction. This strong HC chemisorption is the cause of the large self-inhibiting effect on HC oxidation[58]. Experiments by Voltz yielded rate equations, listed below as Equations 1 and 2, based on the dual site mechanism. Negative reaction orders represent the competitive adsorption processes described above[66].The kinetic model shows good approximation of simulated and real exhaust oxidation experiments, although the HC oxidation performance was only

modeled for the first 80% conversion, corresponding to the easily oxidized fraction of HCs in real exhaust.

$$r_{C_3H_6} = -\frac{k_{r_2}(C_3H_6)(O_2)}{R(\theta)} \quad (1)$$

$$R(\theta) = \left[1 + k_{a_1}(CO) + k_{a_2}(C_3H_6)\right]^2 * [1 + k_{a_3}[(CO)(C_3H_6)]^2[1 + k_{a_4}(NO)^{0.7}] \quad (2)$$

Particle size also influences catalyst activity. In an early study of propylene oxidation, Carballo and Wolf[67] examined the effect of Pt particle size on the reaction rate through kinetics and catalyst characterization by H_2 chemisorption. They found reaction rates increased with propylene concentration to a certain point (maximum conversion), after which the activity decreased, such that at a very high propylene concentration the reaction rate is zero order with respect to propylene. As well, the specific reaction rate increased with Pt crystallite size[67]. However, as with CO oxidation[68], the global reaction rates were highest for smaller particles. The increase in specific activity with particle size indicates that the sintering damage causes more reduction in area by particle agglomeration than by encapsulation in the support[67], in keeping with other studies with Pt supported on a nonporous alumina film[69] and alumina spheres[70]. The related work of Altman and Gorte[71,72] suggested that differences in the Pt crystal planes established for different Pt particle sizes could affect CO adsorption on the surface, and the commonality between CO and HC oxidation (reaction mechanism and inhibition effects) infer that a similar principle may apply for HC oxidation.

A study by Parega et al[73] indicated that changes occur to the Pt particles in oxidation reactions in the presence of trace oxygen, with some crystal edges changing to facets. While the results differ from those recorded by others, Carballo and Wolf[67] attributed

the differences to pre-treatment and reaction conditions, and determined that these effects were in some qualitative agreement with literature[58,64,66,74]. However, their data did not follow the simple bimolecular Langmuir-Hinshelwood kinetic mechanism, suggesting that a more complicated reaction mechanism is required[66,67].

During temperature programmed oxidation experiments with propylene, the reaction lit-off at the catalyst outlet[75]. This occurs because low levels of propylene oxidation occur in upstream portions of the catalyst, and the generated heat is transported downstream by convection. This allows heat to accumulate at the catalyst outlet faster, relative to other axial positions on the catalyst, such that the outlet is the first location to overcome the kinetic limitation of propylene poisoning (discussed above). After light-off, conduction of heat along the catalyst to upstream positions causes the reaction zone to move from the outlet to the catalyst inlet, in a "back-to-front" ignition pattern, which has also been observed by other researchers[76-79]. However, at sufficiently high temperatures, the propylene reaction zone is located at the inlet of the catalyst instantaneously as predicted by Oh and Cavendish for CO oxidation on Pt/alumina pellets[80]. In general, gradients in temperature and concentration waves form over the catalyst monolith, such that the reaction rates are not uniform across the entire surface, which can lead to non-uniform use of the catalyst, and thus non-uniform catalyst damage[75].

2.3 Thermal Deactivation

Typically, simulated thermal degradation is achieved with a homogeneous, or uniform, catalyst aging method (the temperature along the catalyst is kept constant). For example, in a previous study targeted for DOC applications, C_3H_6 oxidation was used

as a probe reaction to study temperature patterns along a monolith-supported Pt/Al_2O_3 catalyst before and after homogeneous thermal degradation[75]. After homogeneous aging, larger temperature rises occurred at locations farther from the front of the catalyst, while the fresh catalyst formed reaction zones closer to the inlet with smaller temperature rises. Another effect was a longer time for the reaction to propagate from the outlet to the inlet portion of the catalyst.

Despite the wealth of knowledge gained from homogenous aging studies[26,36,70,81], degradation is often non-uniform, occurring more at the inlet portion of the catalyst and causing different Pt sintering behaviour than homogeneous aging[82]. Zotin and colleagues found that the upstream portion of a Pd-Ni catalyst in a bench engine setup experienced more degradation, both chemical and thermal, than the middle and outlet positions[83]. Beck studied aging of both Pd and Pd/Rh catalysts in a vehicle exhaust train and saw similar behaviour, even after removing poisons from the surface. The light-off temperatures for CO, hydrocarbon, and NO oxidation increased after aging, especially under stoichiometric oxygen conditions[84]. Conversely, Lambert noted that a DOC experienced a large relative surface area loss at the DOC outlet after aging in an engine dynamometer, and proposed this was due to the damage caused by the exotherms that occur in the back of the catalyst[85]. As well, the light-off temperatures for a sample from the DOC inlet were lower than those from the outlet. Emissions tests indicated that while light-off temperatures increased, hydrocarbon and CO emissions targets were still achieved. These results suggest that heterogeneous aging conditions do occur and that depending on those conditions, different parts of the catalyst will be affected.

Recently, there has been interest in zone-coated catalysts[80,86-89], where for DOC applications, different platinum loadings would be used at the inlet and outlet regions of the catalyst monolith. Non-uniform precious metal distribution minimizes Pt levels used while still meeting emissions targets or targeted NO, CO, and/or hydrocarbon conversions, and possibly improving cold-start emissions. While some of the above literature discussion suggests that thermal degradation at the catalyst inlet may have a larger impact on the performance of a catalyst with higher Pt loadings at the inlet portion, model predictions by Gavriilidis indicate that despite the higher relative loss of active site surface area in the upstream portion of a zone-coated catalyst, the remaining active area would be sufficient to catalyze the reactions and create the required exotherm[86]. As an example, in one simulation the model showed that the uniformly coated catalyst requires 70% of the original activity to generate enough heat for ignition, while the zone-coated catalyst generated the same amount of heat with only 30% of the original activity.

Overall, literature results demonstrate that gradients in reactivity exist along these catalysts, and that typically, the characteristics of the front portion of the sample play a significant role in overall performance. A full understanding of these evolving gradients is critical in tailor-designing catalysts with active site gradients for optimal performance. However, activity gradients caused by non-uniform catalyst distribution due to heterogeneous thermal degradation have not been investigated.

2.4 Sulphur Degradation

Sulphur species in the exhaust originate from sulphur bound in hydrocarbon fuel species, such as thiophenes, which is released as SO_2 during fuel combustion. Before

mandated reductions, unleaded gasoline contained nominally 300 ppm organic sulphur, which one estimate says produced approximately 20 ppm SO_2[90]. Estimates suggest that 5 weight-% of the sulphur introduced via the exhaust is found on the catalyst, with 1-3% in the particulate matter[2]. In recent years, the limit for diesel fuel has been reduced to the ultra-low sulphur diesel (ULSD) standard of 15 ppm sulphur in Canada[91].

Of the various poisons that exist for DOCs, sulphur represents the largest quantity of poison found in used emissions catalysts and is one of the easiest poisons to study using simulated aging techniques[37]. Sulphur is found down the catalyst length[36,92] and into the washcoat depth[7,36]. However, heavier sulphur deposits have been found at the inlet[92]. It is expected that sulphur damage will occur in a plug-like fashion such that the inlet has more sulphur deposited than downstream positions[93]; this property has also been exploited by using sulphur trap components to protect downstream catalysts[94].

SO_2 in the exhaust is further oxidized to SO_3 over the oxidation catalyst in lean exhaust (oxygen rich) at temperatures above 300°C[95,96], with SO_3 remaining stable to temperatures over 700°C[97]. SO_3 is also very acidic, and can react with basic components in the washcoat, such as ceria, or combine with water vapour in the exhaust to form sulphuric acid, which acts to increase PM[2,4,8,98]. Both SO_2 and SO_3 can act as a catalyst poison. The sulphur species, particularly SO_3, migrate preferentially from the precious metal to a sulphating support, which is a support that accepts sulphur species as sulphites and/or sulphates[99-103]. For Al_2O_3-based catalysts, these aluminium sulphates ($Al_2(SO_4)_3$) are a considerable source of deactivation for DOCs[104-106]. SO_2 retention by alumina depends on the surface area and phases of the support, with lower surface area adsorbing less SO_2[107]. SO_2 adsorption on the washcoat increased with time-on-stream[107,108], but the amounts adsorbed decrease as temperature increased[96,99].

Further, Takahashi et al[93] found that for NO_X storage/reduction catalysts, the decrease in NO_X storage depended on the total sulphur exposure and not the actual concentration of SO_2 in the feed. These results suggest there are issues with limiting sulphur poisoning using a temperature-based approach.

Exposure to sulphur can cause changes in catalyst morphology, structure, and electronic properties[107,109-114] which diminish the catalyst activity for CO and HC oxidation reactions[2,90,100,115,116]. The results of these changes might include interfering with the associative adsorption mechanism used by these compounds[90,100] and increased competition for active metal sites[115,118]. There is also evidence that catalyst sulphation induces migration of Pt particles, and others have noted agglomeration following sintering even at lower temperatures, i.e. 200-250°C, in the presence of sulphur[29,111,119]. Sulphur poisoning of the support can also affect the metal-washcoat interactions; for example, pre-oxidized Pt/alumina interacts with SO_2 at the Pt-O-Al interface to reduce Pt and so destabilizes small Pt particles[111].This occurs when the sulphur species form strong bonds with the active metal sites so the resulting surface metal sulphides are very stable and block the active sites for reactant oxidation[109,110].

As aforementioned, propylene oxidation, as well as oxidation of CO and other reactive hydrocarbons, are inhibited by SO_2 over sulphating supports and Pt[90,110,116,115], possibly by interfering with the associative adsorption mechanism used by these compounds[90,100], most likely by competitive adsorption with SO_2 for active metal sites[118]. A different sulphur deactivation mechanism requires high propylene coverage of the Pt surface, such that surface oxygen is low, facilitating SO_2 dissociation[115]. While the oxygen adatoms are used for oxidation, the sulphur adatoms remain adsorbed on Pt active sites, causing deactivation[115]. These sulphur species can be removed very

slowly by the low surface oxygen concentration. This type of deactivation increases with temperature, possibly because the dissociation of SO_2 increases with temperature[115].

Regeneration from sulphur, a process termed desulphation, can recover some of the catalyst activity. For example, catalyst reduction with high temperature and a reducing agent, such as H_2, can remove some of the surface sulphur species for partial restoration of activity[95,117,120]. As SO_2 adsorption on Pt decreases with temperature, in Pt/Al_2O_3 catalysts the most common poisoning component is aluminium sulphates. $Al_2(SO_4)_3$ decomposition was noted by Neyestanaki et al[36] to be thermodynamically possible above 650°C in an oxygen-rich environment (O_2:SO_2 of 10:1), while lower temperature regeneration with a strong reducing agent (H_2) is possible[97,114,120,121], although Jones et al[119] found H_2 regeneration of sulphated Pt catalyst insufficient for methane activity recovery, and also noted Pt agglomeration following regeneration at temperatures below where sintering normally occurs (650°C)[36]. However, desulphation was not able to recover the initial pre-exponential factor, indicating that changes to the support structure occurred when sulphur is added that cannot be undone by removal of sulphur species from the surface[117].

2.5 Spatial Resolution

Several studies have attempted to characterize temperature and reaction gradients with DOC-type catalysts. Sharma and coworkers[122], studying CO oxidation, found that the reaction zone shifted forward toward the catalyst inlet following a step concentration increase, and a zone shift downstream following a step concentration decease; the step increase also reduced the time to reach steady state when ignition had already occurred.

Temperature hysteresis and wrong way behaviour, a phenomenon where a decrease in feed temperature leads to a temperature rise downstream in the catalyst, were also observed. Sun et al[123] also observed hysteresis during CO oxidation of ignition and extinction temperatures on Pt. Feed concentration perturbations shifted the position of the reaction zone within the monolith, with the magnitude of the concentration steps affecting the width of the reaction zone as well as velocity of the temperature and reaction light-off waves to the catalyst inlet[123]. Wrong-way behaviour was also observed by Jaree et al along with other reaction propagation changes[124] and feed perturbation amplification over an inhomogeneous catalyst bed[125]. The switch from slow reaction/diffusion control regimes to active site blocking and coupled heat effects, including heat of reaction, convection and conduction were used by the authors to explain this behaviour.

Spatially-resolved capillary inlet mass spectrometry (SpaciMS) is a gas-phase species concentration measurement technique developed by Partridge et al at Oak Ridge National Laboratory in collaboration with Cummins Inc to study the complex dynamic chemistry occurring within monolith catalysts. Specifically, Partridge and coworkers have used this technique successfully to decouple the complicated chemistry occurring within NO_X storage and reduction monolith-supported catalysts[126-129].

Infra-red thermography (IRT) is a temperature measurement technique that uses the infra-red emission signature from the catalyst to calculate the temperature along the surface. In particular, this technique allows researchers to monitor the temperature patterns in a broader and more dynamic sense than what is achievable with a number of thermocouples. For example, reaction propagation waves and local hot spots can be seen with IRT. Luss et al[79] have used IRT to study temperature gradients along a soot

filter during soot combustion on a monolith DPF. These researchers noted back-to-front ignition[76,78,79] as well as front-to-back ignition of the soot, depending on the steady-state inlet temperature conditions.

Shakir et al[75] combined the use of SpaciMS and IRT to observe propylene oxidation occurring over a Pt/Al_2O_3 monolith-supported catalyst. Light-off at the outlet followed by back-to-front ignition was also observed, with the time for the back-to-front ignition wave to move to the inlet increasing following homogeneous thermal aging.

Overall, literature results demonstrate that gradients in reactivity exist along these catalysts, and that typically the characteristics of the front portion of the sample play a significant role in overall performance. A full understanding of these evolving gradients is critical in tailor-designing catalysts with active site gradients for optimal performance. However, much of the simulated aging has focussed on homogeneous (uniform) damage to the catalyst, which is unlikely to occur in a vehicle exhaust system. In this thesis, a model DOC was tested before and after heterogeneous (non-uniform) thermal and sulphur damage steps. The heterogeneous aging generated more damage at the front portion of the sample to better simulate what might occur in practice.

Chapter 3: Experimental Work

A custom-designed reactor for infra-red thermography (IRT) measurements was used in this study, which is described in a schematic in Figure 1 and a picture in Figure 2. The stainless steel reactor is essentially two metal plates that lie horizontally. The 50 mm x 50 mm catalyst sample is held between the base plate and a sapphire window that was transparent to appropriate IR radiation wavelengths for the FLIR Merlin IR camera used. Thermabraid® GRAFOIL flexible graphite braided packing was placed in a groove located around the reactive section in the bottom steel plate. This product can provide a gas-tight seal when compressed by the 14 bolts around edges of the reactor; a torque wrench was used to ensure equal pressure at all points. The sapphire window is held in place and sealed using 3M Interam expanding insulation, as well as a steel retaining ring bolted to the reactor body to provide more pressure on the window and maintain the seal. The gas enters and exits the catalyst via 6.25 mm (0.25 in.) diameter steel tubing and tapered gas chambers, and flow along the long axis of the reactor. The top plate has a thin groove set at the reactor outlet to guide the mass spectrometer silica capillary through the reactor to the catalyst.

The reactor feed of simulated exhaust gas, comprised of component gases supplied by Praxair, except for the balance N_2 which was generated from air using an On-Site N_2 gas generator, and controlled with Bronkhorst mass flow controllers, was combined upstream of the reactor and passed through a preheater before entering the reactor. Water was passed through an evaporator and introduced just before the preheater. Thermocouples were located at the reactor inlet and back of the catalyst for calibrating/validating the IR camera data, but were not routinely used for analysis. The

composition of the reactor outlet gas stream was analyzed using an MKS MultiGas2030 FT-IR at an acquisition rate of approximately 2 Hz. A Hiden HPR20 mass spectrometer equipped with a custom-designed rig enabled spatially-resolved gas-phase concentration measurements within a channel of the catalyst monolith, a method referred to as spatially-resolved, capillary inlet mass spectrometry (SpaciMS). Inlet and outlet lines were heat-traced and insulated to prevent water condensation.

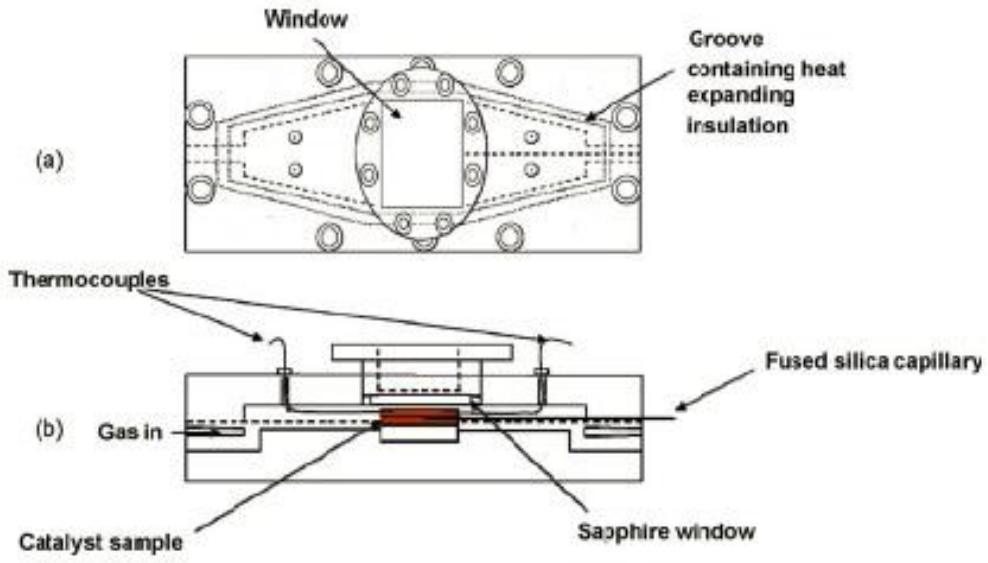

Figure 1. Schematic of the reactor; (a) top view and (b) side view[75].

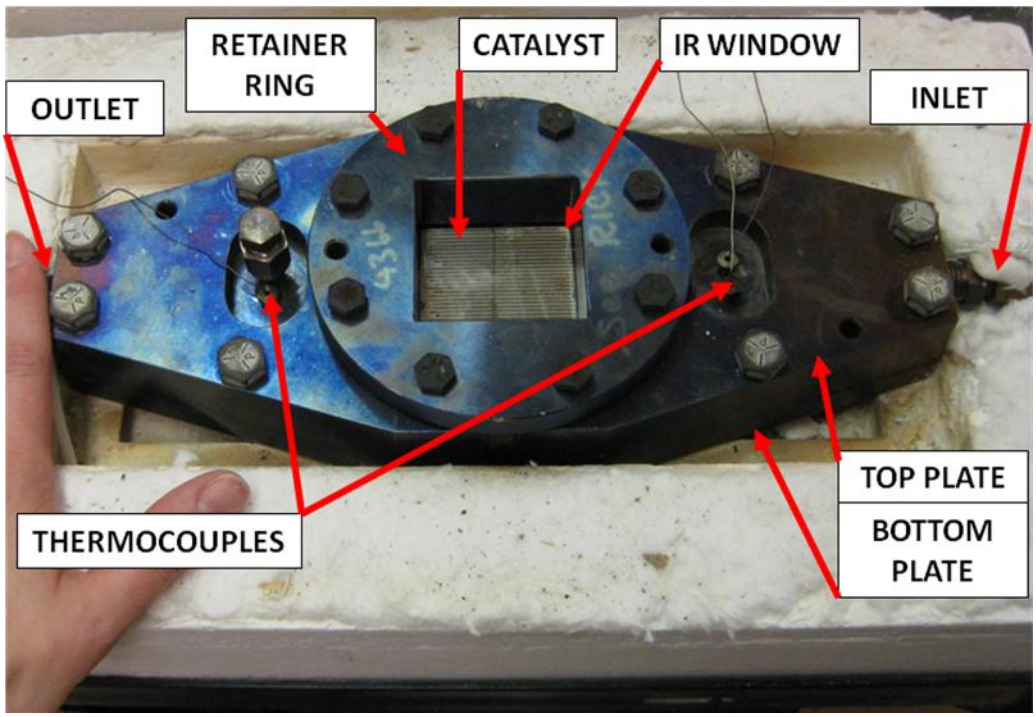

Figure 2. Top view of the IRT custom reactor.

The Pt/Al_2O_3 model catalyst sample, provided by Johnson Matthey, was cut from a monolith block to 50 mm long, 50 mm wide and 7.5 mm thick; two samples were used in this study for the two different heterogeneous aging phenomena tests. The monolith had a wall thickness of approximately 0.25 mm and a cell density of 300 cells per square inch. The Al_2O_3 loading was 1.63 g/in^3 and the Pt loading was 49.9 g/ft^3. A FLIR Merlin Mid InSb MWIR (mid-wave Infra-Red) camera fitted with a FLIR 50 mm lens was mounted vertically above the reactor and imaged the flat surface of the catalyst through the sapphire window. During aging protocols, an optical filter was used with the lens to capture temperature data over 500°C. The FLIR Merlin camera has a focal plane array of detectors such that 320 x 256 temperature points were measured, with the sample covering 200 x 200 of the points, providing a measurement resolution of 0.25 mm. The energy data collected by the camera was converted to

temperature values using ThermaCAM Researcher software made by FLIR Systems Inc. The data are stored as a sequence of frames that make up a movie file, with each frame an IR image comprised of the matrix of temperature values. The data were extracted from the movie file along a line 25 mm from each side of the sample, approximating the radial center position referred to for cylindrical samples. In most cases, nine equally-spaced points along the length, as shown in Figure 3, were used for analysis. Extra positions for data extraction were selected when greater resolution was desired.

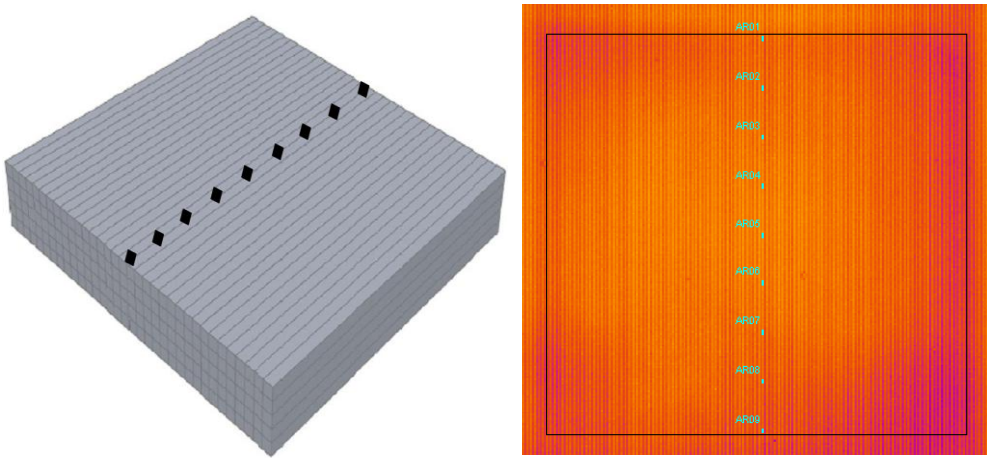

Figure 3. Schematic of data point distribution and an IR camera image (catalyst outlined in black)[130].

In the set-up used in this study, the SpaciMS system consisted of an extended silica capillary, attached to the mass spectrometer with a zero dead volume fitting, which can be moved within a monolith channel to analyze gas species at different locations. The capillary was installed in a central monolith channel to simulate the radial center.

For both deactivation modes, the same experimental methods were used. Each sample was tested in the fresh/unaged condition to establish baseline performance. For both thermal and sulphur deactivation, temperature programmed oxidation and steady-state inlet temperature oxidation tests were performed with propylene as the HC reactant. The gas composition in the TPO experiments was 4500 or 1500 ppm propylene, 6.5% O_2, 4% H_2O, 300 ppm He, and a balance of N_2. The temperature ramp was ~ 4.5°C/minute. The gas flow rate during this test and the others described below was 8.03 L/min, corresponding to a space velocity at standard conditions of 25,000 hr^{-1}. For the TPO data analysis, an experiment was run in the absence of propylene to obtain the IR radiation signature of the temperature ramp due to heater input. This was then subtracted from the TPO IRT data obtained when propylene was oxidized to obtain the temperature rise related to the oxidation reaction and its effects. Figure 4 shows a sample of the two raw data sets, with the resultant temperature rise curve show in Figure 5; temperature rise is the metric used throughout the thesis. For the steady-state inlet temperature tests, 4500 ppm or 1500 ppm propylene was introduced after the catalyst was at a constant temperature, and gas-phase propylene concentrations measured as a function of catalyst position and time; the remaining gas composition was 6.5% O_2, 4% H_2O, 300 ppm He, and a balance of N_2. The IR camera started recording before the introduction of propylene while the catalyst was at a steady-state temperature, such that the initial temperature value was subtracted from subsequent values to obtain the temperature rise profiles during reaction in a similar way to that of the TPO experiments.

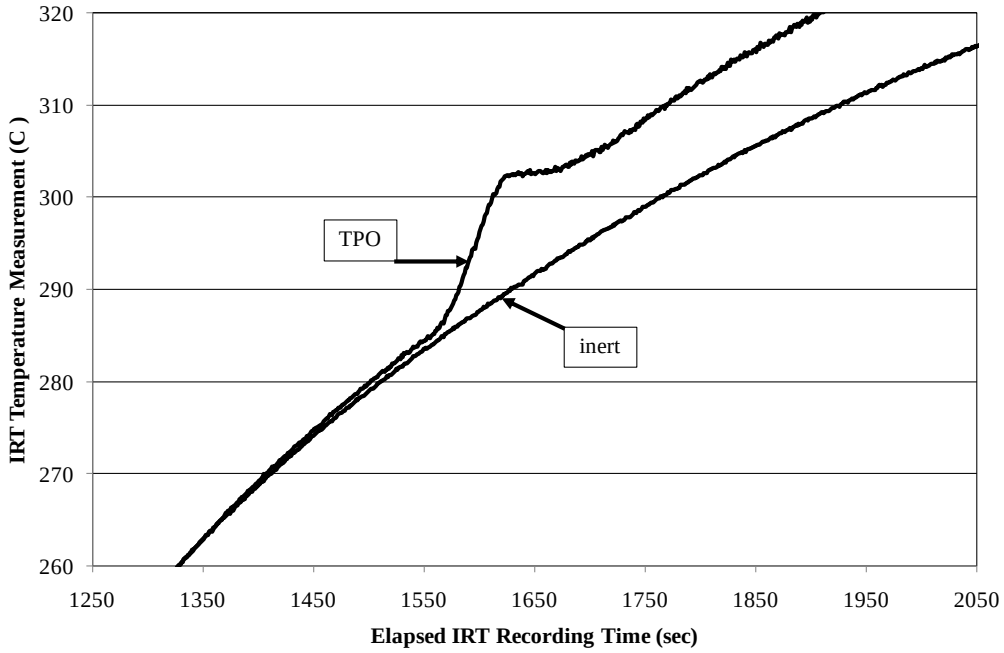

Figure 4. Sample TPO catalyst temperature data sets with and without propylene in the gas stream.

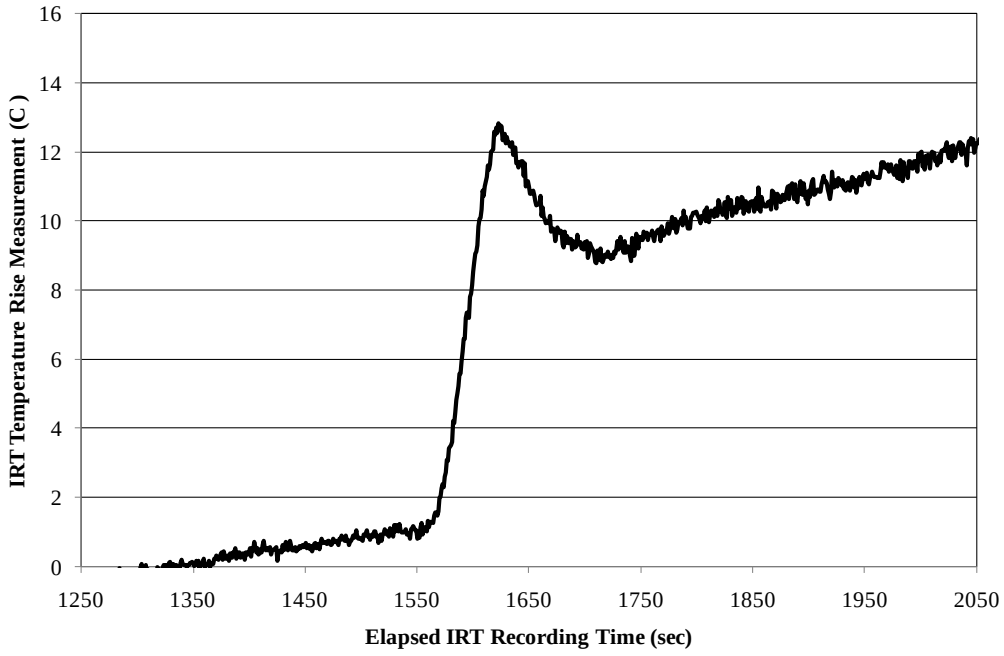

Figure 5. Sample TPO temperature rise profile following subtraction of the inert feed temperature ramp.

3.1 Thermal Degradation

Thermal aging was performed in the reactor, and data will be presented from the catalyst after two aging protocols. To obtain the high, front-localized temperature needed for heterogeneous thermal deactivation, propylene and oxygen were pulsed into the reactor with the catalyst at approximately 500°C. The exothermic oxidation reaction then increased the temperature at the front of the catalyst. To control the absolute temperature increase and how far into the catalyst the temperature rises occurred, the propylene and oxygen were pulsed into the reactor, with an inert phase between such pulses. The active aging pulse contained 13% O_2, 4% H_2O, and the indicated amount of propylene in a balance of N_2, while the inert phase contained 4% H_2O and N_2 only. In the first aging cycle (hereafter referred to as A1), the reactive aging pulse lasted 20 seconds and contained 2.4% propylene. A 10-second "inert" phase was used in between the propylene-containing pulses to avoid extensive heat conduction down the monolith. Ultimately, this technique resulted in the front 12.5 mm of sample reaching temperatures above 650°C for a total of one hour. Sintering of Pt can occur at temperatures over 600°C[36], with higher temperatures causing more severe damage. A segment of the first aging protocol is shown in Figure 6, demonstrating that the catalyst temperature exceeds 650°C in the first 12.5 mm. Although the back of the catalyst was heated above the 500°C set-point during this procedure, the absolute temperature attained at the back portion was significantly lower than that at the front. For the second aging protocol (hereafter referred to as A2), the active phase with 2% propylene was pulsed for 20 seconds, with an 8-second inert phase. This resulted in temperatures over 650°C up to 25 mm into the catalyst and this series was run such that 650°C was maintained in that upstream region for three hours.

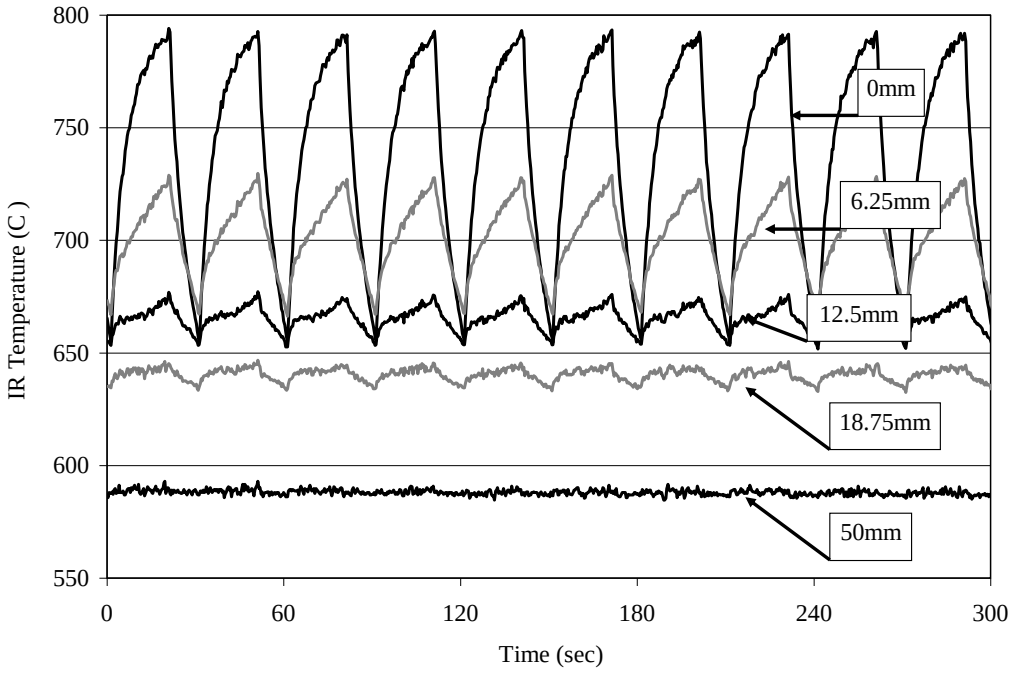

Figure 6. Example temperature data set obtained during heterogeneous aging (A1).

To examine the effect of Pt sintering, dispersion measurements were obtained from the unaged sample and from a separate catalyst sample after aging at three temperatures in the range achieved during pulse aging; dispersion, which measures the ratio between Pt particle surface area to volume, was measured using pulsed H_2 chemisorption with a Hiden Catlab system. The samples were obtained from the same full-size monolith that the sample described above was, and were aged in a standard lab furnace in lab air. These values should be viewed as comparisons between the temperatures rather than absolute dispersion measurements for the samples aged in the reactor. The nature of the heterogeneous aging process makes precise dispersion measurements at each location difficult because each portion of the catalyst length is exposed to a different temperature. Table 1 lists the dispersion measurements obtained after lab aging at different temperatures, with those temperatures representative of measured values

observed during the first aging cycle, and also shows the location where these temperatures are reached during the two aging conditions. In particular, 660°C occurs over twice the amount of catalyst in the A2 aging cycle compared to the A1 cycle.

Table 1. Summary of Temperature Exposures during Aging and Representative Sample Dispersion Measurements.

Aging Temperature (°C)	Location of Temperature (mm)		Dispersion (%) After 1hour oven-aging
	Catalyst A1	Catalyst A2	
Fresh Catalyst	-	-	4.40
660°C	12.5	25	3.69
720°C	6.25	6.25	2.47
790°C	0	0	1.05

3.2 Sulphation

Sulphation was also performed in the reactor, and data will be presented from the catalyst after five aging protocols. To obtain the front-localized sulphation, a reactor feed of 200ppm SO_2, 6.5% O_2, and 300 ppm He in balance N_2 was passed through the catalyst at approximately 375°C. This temperature was chosen based on tests showing that at 300°C, nearly complete oxidation of incoming SO_2 over the same Pt-based catalyst was achieved. The MS capillary was located at different inlet positions to determine when the sulphur reached the desired position, at which point SO_2 was removed from the feed stream. This sulphation method is based upon the assumption that SO_2/SO_3 travels through the catalyst length in a plug, such that no sulphur reaches downstream locations until preceding sites are sulphated. Table 2 summarizes the sulphur exposure location and approximate duration, and also denotes the catalyst designations that will be used throughout the thesis. Measurement of the catalyst

sulphur uptake was not attempted because these measurements require destruction of the catalyst sample.

Table 2. Summary of Sulphur Exposure Locations and Durations

Catalyst Designation	Approximate Sulphation Position (mm)	Time to Reach Position (min)
F	-	-
S1	0-7	2
S2	0-12	6
RS2	38-50	-
S3	0-43+	23
DS	0-12*	46**

* denotes the approximate portion of the catalyst desulphated
** denotes the time to reach the peak sulphur release from the catalyst at the DS position

Following the performance tests for the catalyst before and after the first two sulphur exposures (protocols F, S1, and S2), the reactor was opened and the sample rotated 180°, such that the sulphated portion was then located at the catalyst outlet (RS2). This condition might simulate the catalyst state following a partial regeneration process, where high temperatures and/or reducing agents have freed sulphur from the catalyst inlet, only to have it redeposit at downstream locations. The next step (S3) involved nearly complete sulphation of the catalyst; the MS capillary was placed 43 mm from the catalyst inlet, the most downstream position attainable by the SpaciMS system.

To maintain sufficient activity in NO_X storage/reduction (NSR) catalysts, sulphur must be intermittently removed via a process typically called desulphation, which allows catalyst activity to improve relative to the sulphated state. If a DOC is placed upstream

of the NSR catalyst, it will undergo such a desulphation process as well. This is typically achieved by use of a reducing agent such as H_2 and/or with high temperature exposure[36,95,117]. The final condition (DS) was obtained by partially desulphating the catalyst in the reactor. $Al_2(SO_4)_3$ decomposition was noted by Neyestanaki et al[36] to be thermodynamically possible above 650°C in an oxygen-rich environment (O_2:SO_2 of 10:1), while lower temperature regeneration with a strong reducing agent (H_2) is possible[97,114,120,121]. Desulphation was achieved in this study by feeding 1590 ppm H_2 in balance N_2 to the reactor at 400°C. The MS capillary was located at 12 mm from the inlet to capture the SO_2 and H_2S signatures as the sulphur was released. H_2 was removed from the inlet gas after the measured SO_2 concentration started to decrease from the peak value.

Chapter 4: Heterogeneous Thermal Damage – Results and Discussion

Thermal damage on DOCs most commonly occurs as a result of high temperature excursions, such as those generated for high temperature DPF regeneration. The catalyst is thought to experience greater thermal degradation in the catalyst inlet[82] where the temperature excursion is generated. As well, a model by Gavriilidis[86] indicates that the activity of the inlet plays a crucial role in the overall catalyst performance.

4.1 Temperature Programmed Oxidation (TPO) Experiments*

**This material has been adapted with permission from A. Russell, W. S. Epling, H. Hess, H.-Y. Chen, C. Henry, N. Currier, A. Yezerets, Ind. Eng. Chem. Res. 49 (2010) 10311. DOI: 10.1021/ie1005299. Copyright 2010 American Chemical Society.*

The spatially-resolved temperature rise profiles and spatially-resolved gas concentration data are complementary, as demonstrated in Figure 7 (a sample of the combined data sets obtained during a TPO experiment with 4500 ppm C_3H_6). Light-off occurred at approximately 750 seconds, indicated by the sudden conversion increase at 43 mm (near the back of the 50 mm catalyst). The temperature rise at 43 mm likewise rapidly increased at the same time. The peak in temperature rise occurred when complete conversion was attained, as highlighted by the dashed line. As the reaction moved upstream through the catalyst with time, temperature rise peaks are seen at more forward locations, against the direction of gas flow, exhibiting back-to-front ignition.

This behaviour has been seen previously in heterogeneous catalyst systems with exothermic reactions[75,76,78,79]. The propylene conversion at 25 and 7 mm increased at progressively later times, while the temperature waves stay synchronized at these upstream locations, indicated by the dashed lines at 25 mm and 7 mm. After the reaction wave has travelled upstream of a position, the temperature drops slightly because the heat of combustion is now generated at an upstream location. The temperature rise does not fall to zero because conduction and convection of heat from upstream are still occurring. While both the concentration and IRT data show the same trends, less MS data were acquired due to the necessity of multiple experiments to obtain the spatially-resolved mass spectrometry data profiles, whereas only one experiment was required for the IRT data set. As well, these measurement similarities allow the use of the IRT data to better observe/resolve propylene oxidation through the catalyst length. This behaviour occurred for both the thermal and sulphur damaged catalyst samples.

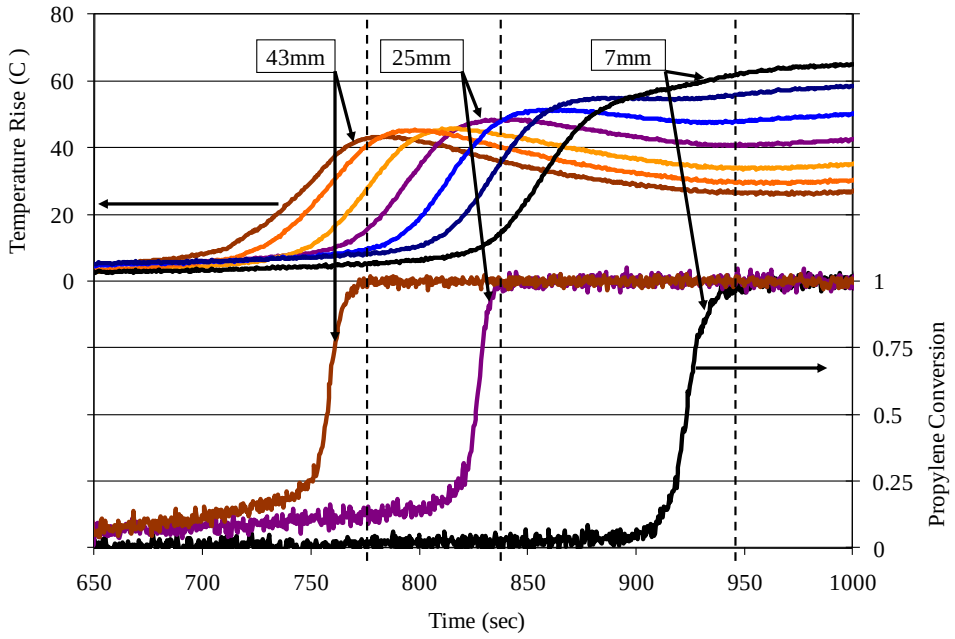

Figure 7. Combined temperature rise and propylene conversion data. Data were obtained from the unaged catalyst, and the gas composition was 4500 ppm propylene, 6.5% O_2, 4% H_2O, 300 ppm He, and a balance of N_2.

With the lower heat of reaction produced by oxidation of 1500 ppm propylene, the profiles are broader and less distinct, with the temperature peak appearing somewhere between 50% and 100% conversion, rather than at 100% conversion found for 4500 ppm propylene. The temperature peak toward the catalyst outlet lies ahead of the 100% conversion mark, but as the wave moves forward these marks come closer, as highlighted by the dashed lines in Figure 8; the 7 mm temperature rise profile starts at temperatures less than 0, but this is only an artefact of the inert temperature ramp subtraction from the oxidation profile.

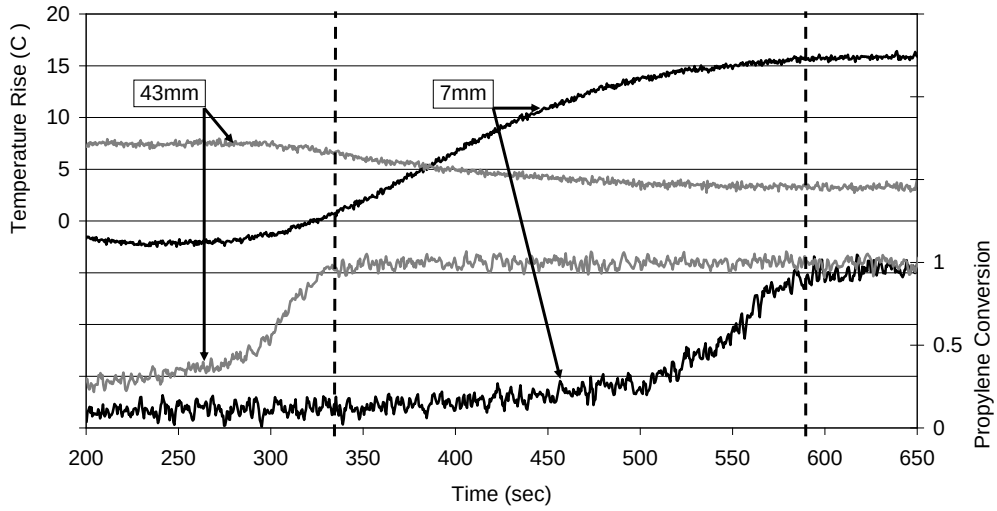

Figure 8. Combined temperature rise and propylene conversion data. Data were obtained from unaged catalyst, and the gas composition was 1500 ppm propylene, 6.5% O_2, 4% H_2O, 300 ppm He, and a balance of N_2.

The thermocouple located upstream of the catalyst and outlet concentration data obtained were used to determine the light-off temperature, here defined as the temperature corresponding to an outlet conversion of 50% (T50), and these values are listed in Table 3 for both 4500 and 1500 ppm. Thermal aging increased the T50 at both propylene concentrations. In all cases, light-off started at the back of the catalyst, instigating back-to-front ignition, as shown in Figure 7. The T50 increase between the fresh and first aged condition is larger than the difference between the two aged conditions, confirming that the damage to the inlet has a significant impact on the catalyst performance.

Table 3. Light-off temperature (T50) of thermally damaged catalyst.

Catalyst Designation	T50 4500 ppm (°C)	T50 1500 ppm (°C)
F	145	127
A1	170	144
A2	180	152

Another interesting observation gathered from the TPO experiments is the change in time required for back-to-front ignition to occur. This can be measured by the MS concentration data as well as the IRT temperature data. The time between 100% conversion being reached at 43 and 7 mm from the inlet are compared to the time between the temperature peaks of 43 and 7 mm in Table 4. The propagation times increased with each aging step for both 4500 and 1500 ppm propylene. As well, in almost all cases the concentration wave travels more quickly than the temperature wave. A few studies have examined the wave traveling behaviour. Yakhnin et al[131] pointed to the interactions between convection, conduction, and heat of reaction causing the concentration and temperature waves to travel at different velocities in packed bed reactors, and the influence of heat transfer rates were discussed by Kulkarni and Dudukovic[132] as key factors in maximum temperature rise and steepness of the temperature wave. The concentration wave may travel more quickly due to the nature of the catalyst outlet, where reaction ignition first occurs. By design of the heterogeneous thermal aging method, the outlet has experienced little thermal deactivation, such that there is still high activity in the outlet. This means the conversion profile for 4500 ppm is very sharp at 43 mm, so the conversion wave moves through the high activity portion quickly. However, the temperature wave is affected not only by the heat of reaction but also the thermal properties of the catalyst (i.e. the same amount of heat must be applied to the catalyst to move the reaction zone

regardless of how many active sites are available for reaction), so the temperature wave moves more slowly relative to the concentration wave.

Table 4. Time between 100% conversion at 43 and 7 mm from the inlet measured by SpaciMS and IRT for thermally aged catalyst.

Catalyst Designation	Δt-100 4500 ppm (sec) MS/IRT	Δt-100 1500 ppm (sec) MS/IRT
F	215/253	280/454
A1	355/389	715/705
A2	390/443	765/900

At the lower propylene concentration, the same pattern was seen. However, the difference between the concentration and temperature wave travel times are much greater at 1500 ppm for the F and A2 catalysts, due to the thermal interactions over that catalyst. With less heat generated by the oxidation reaction with a smaller amount of propylene, the interactions of heat generation and removal are more important. However, the A1 catalyst with 1500 ppm does not follow these trends, with the concentration and temperature waves traveling at nearly the same speed. This catalyst condition may exist very close to a balancing point in terms of heat generation and removal. Furthermore, the A2 catalyst experiences only a small increase in the traveling time for the concentration wave as more of the catalyst is damaged, but the temperature wave moves much more slowly. The lower propylene concentration shows greater effects of aging in both conversion and temperature waves as they move forward in the catalyst.

Another interesting parameter of the TPO experiments is the spatially-resolved temperature wave traveling time. The time was measured using the peak at the back of

the catalyst as the basis, i.e. time was set to zero when the temperature rise peaked at the most downstream position, and the time of each successive temperature peak was recorded. The data obtained from TPO experiments with 1500 and 4500 ppm C_3H_6 before and after aging are shown in Figure 9. The time between peaks increased substantially after the first aging (note that the x-axis is distance from the catalyst outlet, such that the outlet is in the 0 mm position). With 4500 ppm propylene inlet, the second aging (A2) resulted in a curve similar to that of A1. However, with the lower propylene concentration, more significant propagation time differences were observed at the upstream locations of the aged catalyst. The time differences, essentially non-existent in the back 20 mm (0 to 20 mm), are primarily evident at the inlet portion of the catalyst, indicating more significant change at the front of the catalyst, as expected based on the heterogeneous aging method used, and also validating the heterogeneous thermal damage technique. Previous data obtained before and after homogeneous thermal aging also demonstrated increased time between positions after aging, but these increased times were noted through the entire catalyst length[75]. The data in Figure 9 also show that compared to the higher propylene concentration, the reaction zone takes longer to propagate to the catalyst front with 1500 ppm propylene, which is due to the smaller amount of heat generated via the exotherm, making heat conduction upstream slower. This is also likely the reason for more pronounced degradation effects on the time for the reaction zone to move forward for the 1500 ppm propylene experiments.

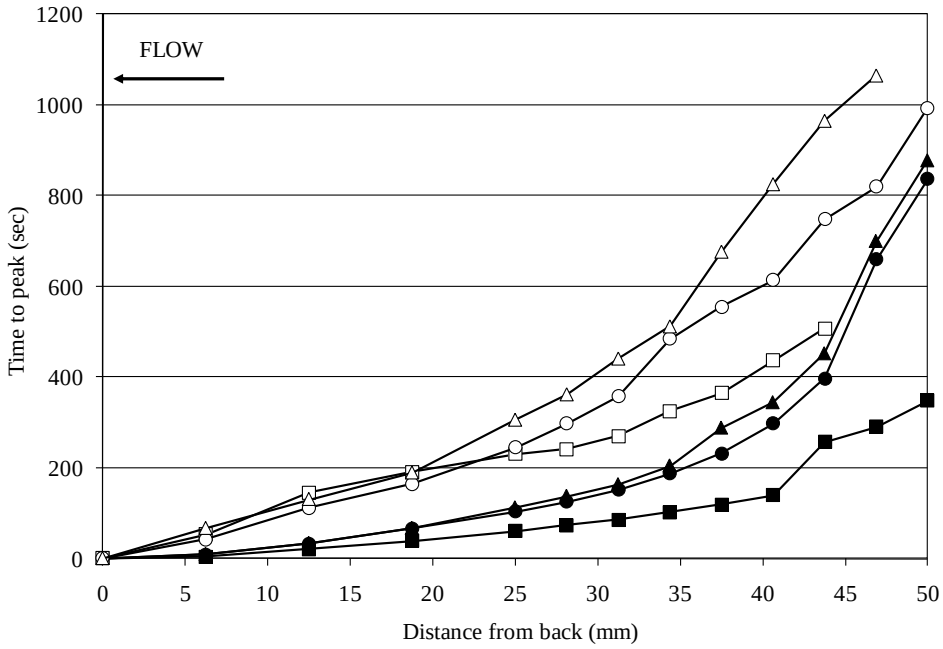

Figure 9. Time between the temperature peak measured at the most downstream position and the temperature peak at different upstream positions, during TPO with 4500 ppm (closed points) and 1500 ppm (open points) propylene. Catalyst F designated by square points (□), A1 by circle points (O), and A2 by triangle points (Δ).

The peak temperature rise values as a function of catalyst position were also compared and are shown in Figure 10 for 4500 ppm propylene. There are three zones to compare, the downstream portion (0 to 20 mm on the x-axis of Figure 10, which is distance from the back of the sample), the middle portion (20 to 40 mm), and the upstream portion (40 to 50 mm from the back of the sample). The temperature rise peak values at the back of the catalyst remain similar even after thermal aging. However, in the middle portion differences become apparent. With each aging, the peak temperature rises in this section are larger. This corresponds to more reaction occurring at those positions, or more specifically, farther from the front, with aging, because less propylene is being oxidized in the upstream portion, allowing more HC to reach the middle. When

considering the upstream portion of the sample, a corresponding effect is seen. The unaged sample experienced the highest temperature rise at the very front, with increasing values between 40 and 50 mm in Figure 10. However, after aging the temperature rise in this region changed slope and decreased, with a drop of ~8°C in maximum temperature observed over the first few mm of sample after the second aging. The same trend is seen with 1500 ppm (not shown), but the effect is less pronounced due to the lower heat of reaction. These data clearly show the effect of the heterogeneous aging. The front of the catalyst underwent degradation, resulting in lower conversion in the very upstream portion before the temperature and concentration waves reached that position. This loss in conversion leads to less heat evolved from the exothermic reaction and therefore less temperature rise observed where the deactivation occurred. These observations of the temperature rise peak pattern correspond to the findings discussed with respect to TPO as well.

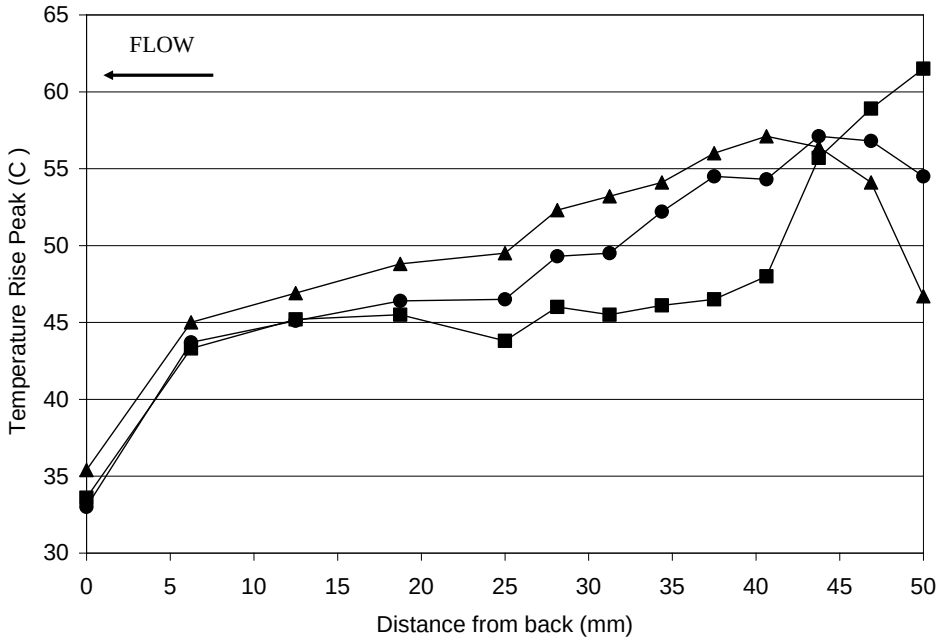

Figure 10. Temperature rise peak values as a function of position from the catalyst outlet, with the gas composed of 4500 ppm propylene, 6.5% O_2, 4% H_2O, 300 ppm He, and a balance of N_2. Catalyst F designated by square points (□), A1 by circle points (O), and A2 by triangle points (Δ).

4.2 Steady-State Inlet Temperature Experiments

Temperatures for the steady-state inlet temperature tests were chosen based on values from the TPO conversion as a function of inlet gas temperature data. Points below and above the reaction light-off zone were chosen, as well as the light-off temperature (T50) measured during TPO on the fresh catalyst. The chosen steady-state experiment temperatures are listed in Table 5 for 4500 ppm propylene. Additionally, common temperatures of 180°C and 207°C were also chosen to increase the number of comparison temperatures. While constant inlet temperature is used for the study, the oxidation reactions themselves are not steady-state; however, the term "steady-state"

will be used to represent these experiments in contrast to temperature programmed oxidations. The effect of aging can be seen from the choice of the temperatures alone, with aged catalysts requiring a higher temperature to instigate light-off (temperature for 50% outlet conversion), similar to the observation of increasing T50 following aging during TPO experiments. This occurs because it takes longer for the catalyst to accumulate reaction heat at the back via convection, and some conduction, from upstream where there are low levels of reaction. This amount of heat generated in these upstream portions is reduced by thermal degradation, and so higher temperatures are required for the same performance.

Table 5. Steady-state oxidation test temperatures for 4500 ppm propylene

	Fresh Catalyst	A1 Catalyst	A2 Catalyst
Below light-off	133°C (not shown)	145°C (not shown)	170°C
50% Conversion	145°C	170°C	180°C
Above light-off	233°C	233°C	233°C
Common	180°C 207°C	180°C 207°C	207°C

Conversion profiles as a function of position, referred to as reaction zone profiles, were generated for various steady-state inlet temperatures and aging conditions for the oxidation of 4500 ppm propylene and are complied in Figure 11. Measurements were taken when steady-state had been achieved, as determined by the outlet concentration measured by the FTIR being constant. The time to reach steady state was not considered. The reproducibility of these measurements is studied in Appendix A. With the fresh catalyst, the reaction zone was similar at all steady-state inlet temperatures beyond that where light-off would occur spontaneously, i.e. at approximately 145°C,

and full conversion occurred within the first 5 mm of sample. Not shown is the conversion profile obtained at the lowest temperature tested, 133°C, where there was simply a linear increase in conversion along the catalyst length to a maximum of 10% at the outlet. At this low temperature, the conversion reached a steady-state value of less than 100% because the heat from the reaction exotherm was not sufficient enough to overcome convective losses and drive light-off.

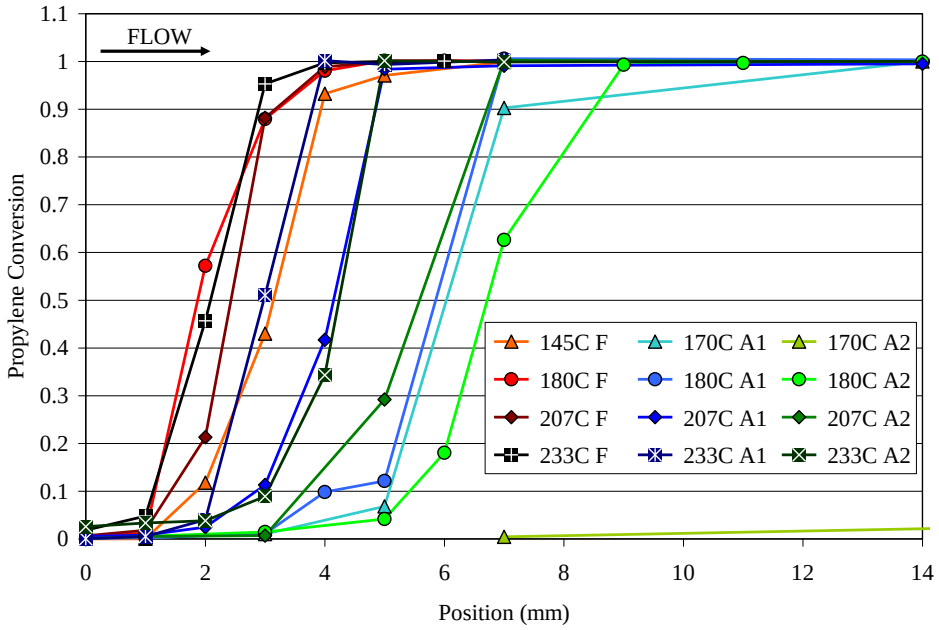

Figure 11. Steady-state, spatially-resolved conversion profiles over the first 14 mm of catalyst. The gas composition was 4500 ppm propylene, 6.5% O_2, 4% H_2O, 300 ppm He, and a balance of N_2. Note that the x-axis is now relative to the upstream face (0 mm is the catalyst inlet).

After the first aging process (A1), the reaction zone shifted downstream by 1 to 3 mm for the higher temperatures (180°C, 207°C, and 233°C). At temperatures above 170°C (full light-off temperature for A1), the reaction zones were no longer in similar

positions, in contrast to the fresh sample where all the reaction zones were in the same catalyst region of 1 to 3 mm. For example, the reaction zone of A1 catalyst at 233°C is approximately 1 mm upstream of that at 207°C. It is also apparent that the zone widened slightly, as the reaction zone width is approximately 2 mm for all temperatures on the fresh catalyst, and 2 to 4 mm after the first aging. As previously mentioned regarding Table 5, while the fresh catalyst lit-off at an inlet steady-state temperature of 145°C, catalyst A1 had negligible conversion at 145°C (not shown), and ultimately achieved light-off at 170°C. Light-off occurs because small amounts of propylene are oxidized generating a small amount of heat which is carried downstream, where it collects and overcomes propylene poisoning[58]. The aged catalyst reacted less propylene in the front section of catalyst, leading to less heat generated by the reaction and therefore less transfer by convection and/or conduction downstream, and as such heat transfer is a fundamental component of back-to-front ignition. This change in exothermic reaction heat production delays the ignition at the catalyst outlet[75]; ignition delay can also be affected by the amount of catalyst or thermal mass downstream that needs to be warmed[133]. The impact of lower catalyst activity in the damaged front portion was less significant at the high propylene concentration because there was still enough propylene oxidized to generate heat that is carried downstream to initiate light-off and back-to-front ignition when the steady-state temperature exceeds the light-off temperature. Further aging (A2) required even higher temperatures for light-off (180°C) and to attain the same reaction zone profile, which is apparent in comparing the profiles of 207°C for A1 and 233°C for A2, which are very similar in location and width. The changes are most significant in the very front portion of the catalyst, indicating that the majority of the catalyst length did not experience significant damage from the heterogeneous aging method, as intended.

Another spatial measurement that demonstrates the changes in catalyst oxidation performance is the location along the axis of the catalyst where the propylene oxidation reaction proceeds quickly to high conversion. This is measured by IRT as a large temperature rise, and will be called the light-off location (in contrast to the previous definition of light-off temperature). Table 6 contains the light-off position in the catalyst by steady-state inlet temperature and catalyst condition. These measurements have a resolution of ~6.25mm from the IRT data; a sample IR light-off plot is shown in Figure 12. In this figure, the position curve of 25 mm rises ahead of those downstream of it (i.e. 31.25 to 50 mm) and reaches its peak temperature rise before those curves of upstream positions; the reported light-off position would thus be 25 mm.

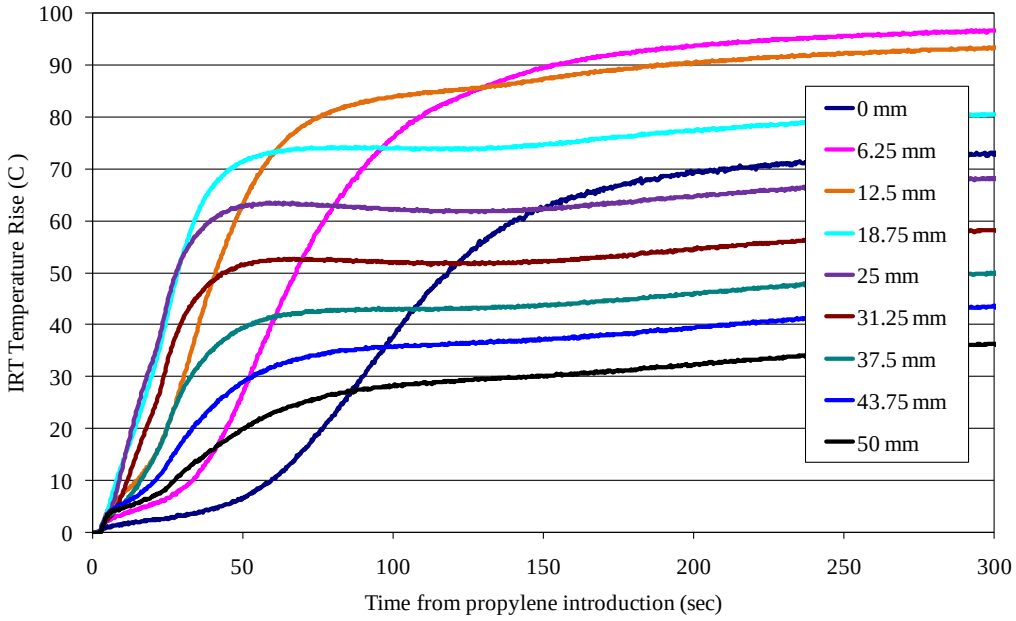

Figure 12. IRT Temperature rise light-off sample. From 207°C steady-state with 4500 ppm propylene, 6.5% O_2 and balance N_2 with the catalyst condition A1.

Table 6. Light-off positions during steady-state experiments with 4500 ppm propylene on thermally damaged catalyst.

	Light-off Position (mm from inlet)		
Steady-State Temperature (°C)	F	A1	A2
145	43.75	None	-
170	-	50	None
180	12.5	43.75	50
207	6.25	25	37.5
233	0	12.5	18.75

These measurements very clearly indicate the light-off position moved downstream from the fresh (F) position as the catalyst was thermally aged (A1 and A2). This light-off position delay occurs because it takes longer for the catalyst to accumulate heat at the back via convection, and some conduction, from the low levels of reaction exotherm in upstream positions where thermal sintering decreased the available active site surface area for oxidation. Heat transfer is an essential component of back-to-front ignition because the collection of heat from upstream exothermic reactions that drives light-off[75]. This was also discussed above during TPO where the smaller amount of heat generation at the inlet after aging delays the ignition at the back. A similar effect occurs at steady-state, but the steady-state temperature may exceed that required to generate light-off, so the ignition can occur upstream of the outlet position. The damaged inlet is not able to generate the heat required to ultimately covert all the propylene, which moves the light-off position downstream as fewer active sites are available and so more of the catalyst is used to achieve the same performance.

These effects of lower heat generation due to less propylene oxidation for the aged catalysts were more prominent during tests with 1500 ppm propylene. The steady-state temperatures tested with 1500 ppm propylene were not the same as those selected for the 4500 ppm propylene experiments, due to different light-off temperatures. Four temperatures (133°C, 145°C, 170°C, and 225°C) were used to compare the three catalyst aging conditions with 1500 ppm propylene. A key difference between the data sets from the experiments with 4500 and 1500 ppm propylene was the formation of "stagnant" steady-state reaction zones (no back-to-front ignition) at different locations in the catalyst for each steady-state inlet temperature, which can be seen in Figure 13. For example, at the lowest steady-state inlet temperature, 133°C, for the fresh sample, the reaction started and remained near the back of the catalyst, while at 145°C ignition occurred and remained in the front half of the catalyst, but did not move closer to the inlet. This might indicate that heat generation and removal, primarily convection, were nearly balanced under these conditions. This contrasts the 4500 ppm propylene observation, where if light-off occurred somewhere other than the very front, back-to-front ignition was observed; otherwise, conversion was, and remained, incomplete. Of further note, light-off did not occur with 4500 ppm propylene at 133°C, while at 1500 ppm full conversion was recorded. This is attributed to propylene poisoning, inhibiting light off at the higher concentration[58].

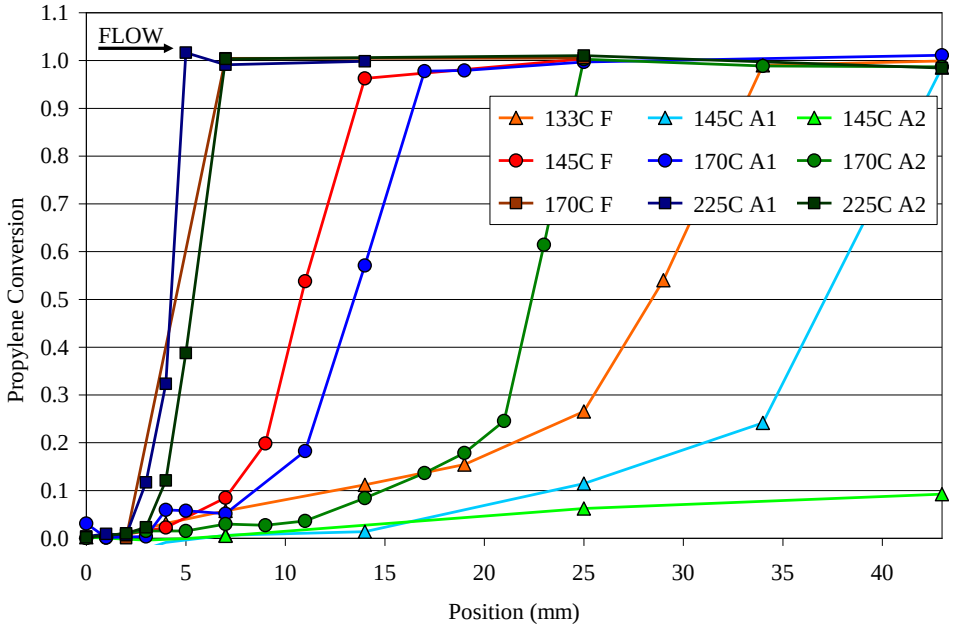

Figure 13. Steady-state, spatially-resolved conversion profiles over the first 43 mm of catalyst (last point measured). The gas composition was 1500 ppm propylene, 10% O_2, 4% H_2O, 300 ppm He, and a balance of N_2.

Again, for the 1500 ppm propylene tests, thermal aging decreased catalyst activity at the catalyst inlet and caused wider reaction zones compared to the fresh catalyst under otherwise identical conditions. For the 170°C steady-state, the width increased from 10 mm on fresh catalyst, to 12 mm on A1 and 14 mm on A2, although reaction zone width increases were somewhat mitigated with very high temperatures. The same stagnant reaction zone behaviour was noted with aged catalysts A1 and A2, although the catalyst damage shifted the reaction zone toward the catalyst outlet. This is especially apparent when comparing the reaction zones of 145°C. The fresh catalyst attained complete conversion by 25mm, while following the first thermal damage cycle complete conversion required the full catalyst length. Additionally, following the second thermal aging cycle complete conversion could not be obtained within the catalyst length.

Similar movements of the reaction zone downstream were seen at 170°C, and to a small extent at 225°C.

There was also a shift in the light-off location downstream, which would be expected from the preceding discussion about stagnant reaction zone movement with aging. For comparison, the light-off location measurements for 1500 ppm are listed in Table 7, with the measurements collected in the same manner described previously. In every case the location shifts toward the outlet with aging, and upstream with increasing steady-state temperature. The exception is 170°C for the fresh catalyst which showed the same light-off position as 145°C because the higher temperature was insufficient to move the reaction zone forward 6.25 mm to reach 0 mm (i.e. the measurement resolution was insufficient to capture the movement of the light-off position between these two temperatures on fresh catalyst). At high inlet temperatures, ignition occurred very near the catalyst inlet.

Table 7. Light-off positions during steady-state experiments with 1500 ppm propylene on thermally damaged catalyst.

	Light-off Position (mm from inlet)		
Steady-State Temperature (°C)	F	A1	A2
133	25	none	-
145	6.25	43.75	none
170	6.25	25	43.75
225	-	6.25	12.5

Chapter 5: Heterogeneous Sulphur Damage

Sulphur, in the form of SO_2, exists in the exhaust gas due to combustion of sulphur-containing hydrocarbons in the engine. Sulphur deposits on the catalyst in a plug-like fashion, such that the inlet section of a catalyst experiences a larger degree of deactivation by sulphur poisoning. As the DOC is typically the first catalyst contacting the exhaust gas, the inlet of DOC is where most of the sulphur is located. Again, the model by Gavriilidis[86] indicated that the activity of the inlet plays a fundamental role in the overall catalyst performance.

5.1 TPO Experiments

The light-off temperature was measured as the reactor inlet temperature when the outlet concentration reached 50% (T50), the same parameter measured for during thermal aging testing. This temperature value increased as the catalyst was exposed to sulphur, which has also been seen with engine-aged catalysts[39,105]. These T50 values are listed in Table 8 by the catalyst condition designator for both the high (4500 ppm) and low (1500 ppm) propylene concentration tests. For the high concentration, the first two sulphations increased the light-off temperature by 10°C. The S2 sulphur exposure is approximately double the catalyst volume of the S1 exposure, suggesting that the sulphur does tend to affect the catalyst as a plug moving from the inlet to the outlet[93]. The difference between the fresh (F) and first aged sample (S1) of 10°C is quite smaller than the 25°C increase in T50 noted for thermal aging between F and A1 catalysts,

indicating that the thermal aging procedure used in Chapter 4 caused much more severe catalyst damage than the sulphur damage procedure discussed here. Of course, different thermal aging conditions will generate different extents of degradation, such that lower temperature exposures will lead to less damage and therefore possibly changing the relative amounts of damage. Therefore, the comparisons made here are specific to the degradation conditions used in this study. T50s also increased for the low concentration, but the measured effect is not as strong because the extent of poisoning by propylene is smaller at the lower concentration.

Table 8. Light-off temperature (T50) of sulphur poisoned catalyst.

Catalyst Designation	T50 4500 ppm (°C)	T50 1500 ppm (°C)
F	155	127
S1	165	144
S2	175	152
RS2	181	158
S3	204	173
DS	191	165

Recall that the RS2 catalyst condition is a rotation of the catalyst S2, such that the sulphur damaged inlet of the S2 catalyst has been relocated to the catalyst outlet, or in other words the undamaged catalyst has been relocated to the inlet. The T50 temperature value for RS2 is slightly higher than S2 because the light-off process during the TPO starts at the outlet position before moving forward in back-to-front ignition. When the sulphur damage is located at the inlet, there is still a large body of the catalyst to generate heat from exothermic oxidation of propylene, and the heat collects at the back, where there are still un-poisoned sites, and can overcome the kinetic limitation of propylene poisoning[58] and some of the sulphur poisoning. However, when the sulphur is located at the outlet, there are fewer un-poisoned sites

available for propylene oxidation at the outlet where heat is slowly building up from upstream oxidation, so the extent of propylene poisoning is compounded and higher temperatures are required to overcome it. When the entire catalyst is sulphated (S3), there is another large increase in T50, for both high and low concentrations. Although the T50 values increase for the low concentration, the measured effect is not as strong because the extent of poisoning by propylene is smaller, while poisoning by sulphur does not change with the propylene concentration.

Following desulphation, the T50 is lower compared to the S3 catalyst, but still higher than those for S1 and S2, indicating that some, but not all, of the activity was recovered with partial removal of sulphur. This is expected since the partial removal of sulphur results in more left on the catalyst compared to the amounts deposited during the S1 and S2 tests, provided that dsulphation occurs in a plug-like fashion as well (i.e. the inlet 12 mm is desulphated, the remaining 38 mm is still sulphur damaged), although direct measurement of the amount of sulphur removed from the catalyst was not performed. Other desulphation tests have shown that in terms of reaction kinetics, the fresh pre-exponential factor was not recovered, indicating that the sulphation process alters the support structure, which cannot be undone by removal of sulphur species from the surface[117] and such an effect may also impact the extent of the regeneration here.

The TPO data also demonstrate that there is a change in time required for back-to-front ignition to occur. As discussed in Chapter 4, this can be measured by the MS concentration data as well as the IRT temperature data because the spatially-resolved temperature rise profiles and spatially-resolved gas concentration data are

complementary, as demonstrated in Figure 7. The time between 100% conversion being reached at 43 and 7 mm from the inlet are compared to the time between the temperature peaks of 43 and 7 mm in Table 9. The times recorded for the 4500 ppm propylene tests for states F, S1, and S2 show a clear increase in time for the temperature wave to propagate from back to front with increasing sulphur exposure, and these three conditions also showed the largest increase in T50. The wave propagation times for conditions F, S1, and S2 at 4500 ppm are in the same pattern and range of those recorded on thermally aged catalyst, indicating that similar patterns of degradation occurred, specifically damage to the inlet portion. The time for RS2 (4500 ppm), however, is about one-third that for S2. Back-to-front ignition occurs more quickly for RS2 because the sulphur damage is located at the outlet, or where time "starts" for ignition, such that the effect of the sulphur cannot be characterized with this metric. This is caused by the longer time taken in the temperature ramp to achieve light-off on the catalyst. After light-off the entire catalyst is at a higher temperature state such that the ignition wave travels more quickly through the undamaged portion of catalyst. Similarly, for S3 the ignition time is only slightly longer than the fresh catalyst because the entire catalyst is at a higher temperature state when ignition begins, so when light-off finally occurs it proceeds rapidly from back to front. As observed during the thermal aging, in almost all cases the temperature wave takes longer to travel than the concentration wave. A caveat of interpreting the time values is that they cannot be examined without considering the changes in T50 previously discussed, because the system temperature is different for each catalyst condition, which affected the wave traveling times. They are still discussed here because the measurements can show important information about the catalyst activity following light-off of the reaction. For example, the S3 catalyst has a temperature wave traveling time of 137 seconds compared to 144 seconds for fresh, which alone might indicate that the S3

catalyst has more activity, but when considered along with a 49°C increase in T50, the fresh catalyst is much more active. However, the wave travels faster over S3 catalyst at the higher temperature, indicating that higher temperatures can mitigate the negative impact of sulphur on the catalyst activity. This was not readily apparent during thermal deactivation tests because even with higher system temperatures, the thermally degraded catalyst cannot achieve the same level of activity as the fresh catalyst. On the other hand, the system temperature was important for the sulphur experiments because the effects of the damage are less significant than those observed previously during thermal deactivation. As such, while the measurements can be quantitatively compared for each type of aging, only qualitative comparisons should be made between the thermal and sulphur damaged catalysts. These observations will be discussed in more detail below.

Table 9. Reaction wave traveling time for sulphur poisoned catalyst.

Catalyst Designation	Δt-100 4500 ppm (sec) MS/IRT	Δt-100 1500 ppm (sec) MS/IRT
F	85/144	401/496
S1	300/323	744/677
S2	341/340	587/553
RS2	110/*	205/225
S3	114/113	237/279
DS	133/137	273/334

*light-off started upstream of 43 mm

When examining the wave traveling times for 1500 ppm in Table 9, the lower concentration results in more deviation between the temperature and concentration measurement. The concentration wave travels slightly slower following inlet sulphations (S1 and S2), while the catalyst damaged in the outlet (RS2, S3, DS), where light-off occurs, shows the concentration waves traveling faster through the catalyst, in

contrast to the sample with sulphur deposited at the inlet. The change in behaviour indicates that the smaller exotherm generated by 1500 ppm propylene results in more balanced interactions between heat generation and removal, which is also indicated by the broader temperature and concentration profiles. The difference between the sample having sulphur at the inlet versus at the outlet results in different "higher activity" locations. When there is higher activity at the outlet (inlet portion exposed to sulphur), ignition occurs in the high activity outlet section, following the normal trend, but as the waves move forward the conversion wave proceeds more slowly through the damaged portion because fewer sites are available for reaction. When the outlet portion is sulphated, more of the active sites are located toward the inlet, so ignition is delayed but the conversion profile can move more quickly through the higher temperature and highly active inlet section once ignition begins, while the temperature wave does not move as quickly due to heat conduction and thermal inertia also playing a role in the IRT data. Further, the wave propagation times are much faster following sulphation than following thermal aging. While there is some impact of the higher system temperature as previously discussed, it is likely that the damage caused by thermal degradation was more severe to the catalyst than sulphur damage. This is noticed at the lower 1500 ppm propylene because the heat generation and removal processes are more balanced, and as such are more sensitive to catalyst changes.

Other than the correlation between the temperature and conversion profiles, the low concentration propylene tests behave in much the same manner as the high concentration. One difference noted, however, is that the time for S2 back-to-front ignition was shorter than for S1. When these two TPO curves are compared in Figure 14, the light-off curves at 7 mm are approximately the same for both, such that both reach 100% conversion around the same temperature, although S1 lit-off at 43 mm at a

lower temperature. This reflects that higher temperatures are required to overcome the lost heat generation in the inlet between S1 and S2, while the damaged inlet portion of the catalyst is not differently affected and they behave similarly.

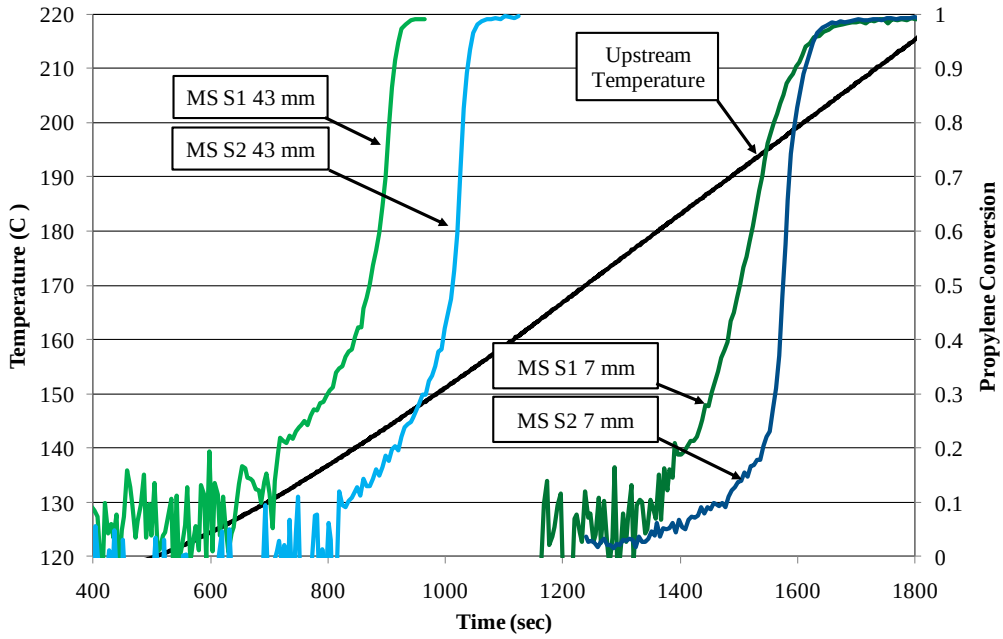

Figure 14. Combined propylene conversion profiles during TPO. Data were obtained from the S1 and S2 catalysts, and the gas composition contained 1500 ppm propylene, 6.5% O_2, 4% H_2O, 300 ppm He, and a balance of N_2.

Not captured in the Δt-100 by concentration measurements is that light-off did not start at the very outlet location for the RS2 catalyst with 4500 ppm propylene, in contrast to all the other sulphated conditions and previous work with homogeneous[75] thermal aging and the previously discussed heterogeneous aging, because the preceding metrics only characterized the temporal data from two locations. The IRT data can be used to better resolve the reaction front, compared to the limited SpaciMS data obtained. The time between successive temperature peaks during back-to-front ignition are shown in Figure 15 for 4500 ppm and Figure 16 for 1500 ppm C_3H_6. While for thermal aging the

temperature peak at the outlet was used as the start point to measure the time between successive temperature peaks as the reaction wave moved upstream in the catalyst, this was not feasible in the present study since RS2 did not light-off at the outlet, and also the large differences in T50 that were noted. Instead, time was measured from the point where the oxidation and inert ramps were aligned for subtraction; the same point was used for all TPO analyses. The same patterns are seen here for IRT as for T50 and Δt-100. When the catalyst was first sulphated (S1), the time required for observation of light-off at the outlet increased. The time curve as the reaction wave moved forward in the back half of the catalyst (0-25 mm from the outlet) is still similar to the fresh catalyst, while the wave travels more slowly upstream of that, which is similar to the heterogeneous thermal aging pattern described above in Chapter 4. However, the thermally aged catalyst showed very little change in pattern between the fresh and aged catalysts downstream of 20 mm, unlike the sulphated catalysts. S2 shows a different curve shape in the middle portion of the catalyst for both concentrations, indicating that as more of the inlet portion of the sample was exposed to sulphur the movement of the wave is changed; more specifically, the travel time slope starts to increase between 12 and 30 mm (from the outlet), while the S1 time starts to diverge more sharply at 30 mm. These positions are farther downstream from the inlet than the approximated sulphation point (43 mm from the outlet for S1 and 38 mm for S2). There are two possible causes for this observation. The first is that SO_2/SO_3 may have penetrated farther into the catalyst after the SO_2 was removed from the feed stream. The second cause is that the presence of sulphur in the catalyst inlet decreased the extent of oxidation there, which means less heat is being moved downstream, thus slowing the reaction wave progression to the inlet. In terms of sulphur migration, while it may be possible that previous tests with high temperatures allowed migration of sulphur

species downstream, sulphur release was not observed from a similar sample in O_2 exposure at temperatures below 500°C[120].

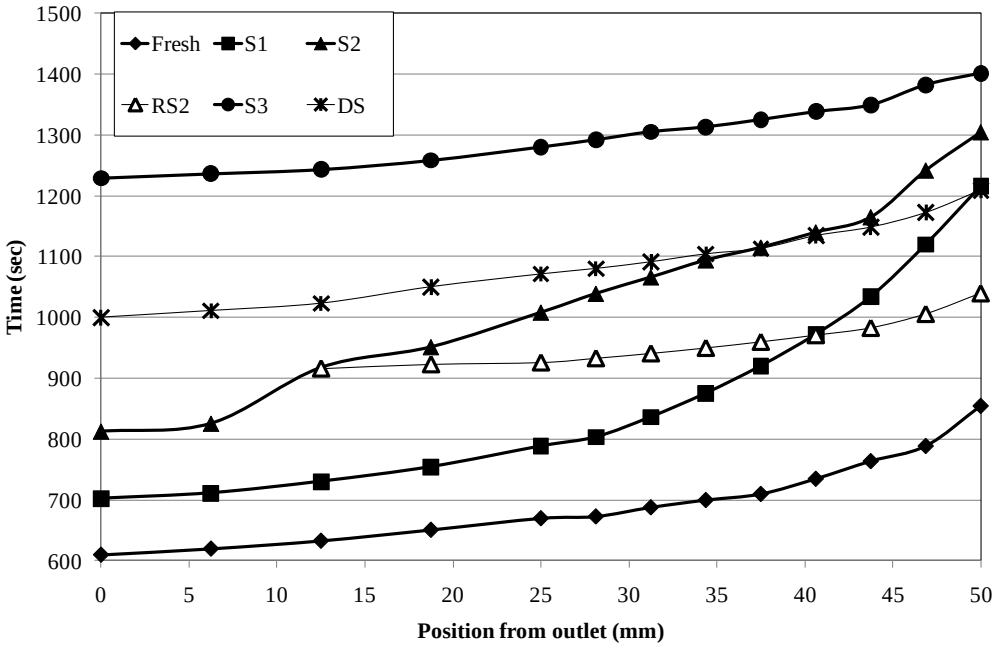

Figure 15. Time between the reference temperature and the temperature peak measured at different catalyst positions. The reactor feed consisted of 4500 ppm propylene, 6.5% O_2, 4% H_2O, 300 ppm He, and a balance of N_2.

RS2 and S3 also show relatively flat time curves indicating the reaction zone is travelling through homogeneous segments of the catalyst, as well as reflecting the higher temperatures needed for light-off to begin, and therefore less time is required for the temperature wave to propagate from back-to-front. Also note that for RS2 with 4500 ppm propylene, light-off commenced at 12 mm from the outlet first, with subsequent temperature rises but no peak, at positions 0 and 7 mm from the outlet, due to heat convection/conduction downstream. Shakir et al[75] observed that after homogeneous thermal degradation, the back-to-front ignition time increased through

the entire catalyst length. This was not seen in the complete sulphation (S3) case for either propylene concentration. While the sulphur damage makes the reaction light-off occur at higher temperature by increasing the amount of heat required to overcome sulphur in addition to propylene self-poisoning discussed above[58], once light-off does occur at the higher temperature, the reaction proceeds more quickly over the hotter surface as the inhibition by propylene poisoning is less significant at the higher temperature; the catalyst seemingly maintains better activity after sulphur damage if sufficient temperatures are used. This was not the case for the thermally deactivated catalyst, which showed progressively longer times were required to move the reaction zone to the catalyst inlet. This comparison simply indicates that sulphation damage primarily affects low temperature performance, whereas thermal damage spans a wider temperature window. After desulphation (DS), the slope of the time curve is similar to S3, but less time was required because the catalyst was more active following the high temperature H_2 treatment that removed some of the sulphur. As well, the slope is similar to S3 because the majority of the catalyst is still in the S3 condition, particularly at the outlet. Very similar patterns were observed with the low propylene concentration experiments in Figure 16, but the time for the temperature waves to travel was longer, although the outlet (0 mm from outlet) ignition starts around the same point in the ramp. This is due to the smaller imbalance between heat generation and removal over the catalyst, and how this balance affects the driving force for back-to-front ignition (i.e. the lower propylene concentration has slower heat conduction upstream because of the smaller reaction exotherm).

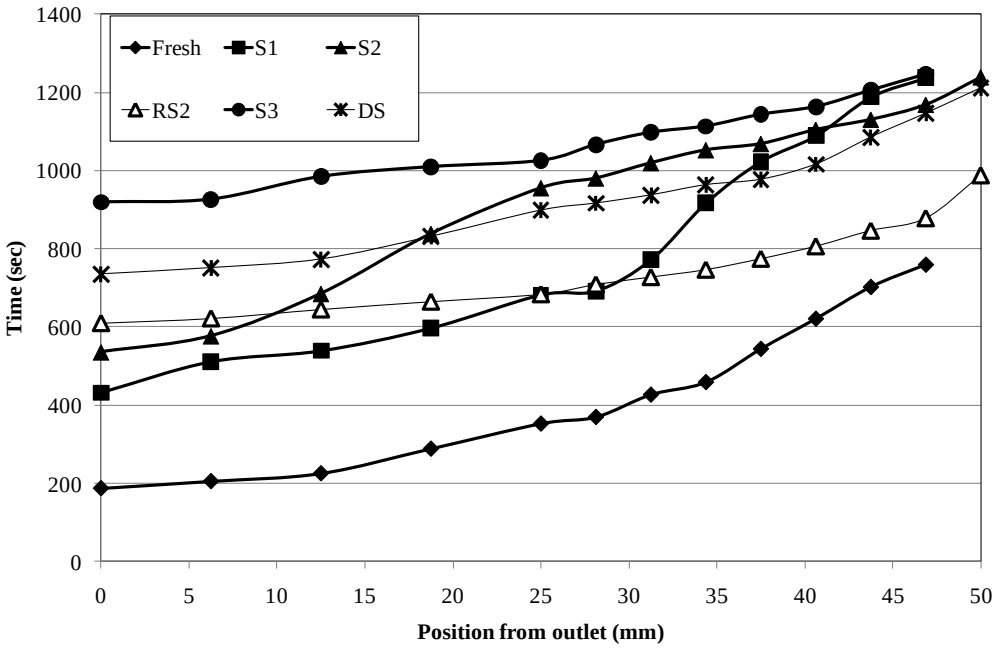

Figure 16. Time between the reference temperature and the temperature peak measured at different catalyst positions. The reactor feed consisted of 1500 ppm propylene, 6.5% O_2, 4% H_2O, 300 ppm He, and a balance of N_2.

The impact of sulphation on the temperature rise peaks that occur during TPO was also examined for 4500 ppm, with results shown in Figure 17. The low concentration tests result in much smaller temperatures rises that are harder to discriminate, and therefore these data are not shown. The large differences in light-off temperature created an uneven basis for comparison, so the compared values are relative to the temperature peak at the catalyst outlet. Although these relative temperature rise peak values do not necessarily reflect overall catalyst performance, they do illustrate features of the light-off patterns that occur over the catalyst. Overall, the magnitudes of the peaks increase from back to front along the catalyst. A larger temperature peak indicates more reaction is occurring at that position, because heat from the exothermic reaction occurring there is added to the heat of convection/conduction. After the first sulphation, higher peaks

are recorded in the front half of the catalyst (25-50 mm) compared to the fresh catalyst, including the sulphated portion (~43 mm from the outlet); however, the slope between 40 to 50 mm from the outlet is fairly flat, indicating that the temperature is not continuing to rise in the damaged inlet. Similarly, following treatment S2, the temperature rises in the12.5-31.25 mm range are larger than the inlet temperature rises, indicating a further shift of the majority of reaction to downstream locations. RS2 exhibits a fairly even-sloped profile between 12.5 mm and 50 mm, but at the damaged downstream portion the recorded temperature rises are much smaller because less propylene is being oxidized. This was seen earlier when the RS2 catalyst did not experience light-off at that catalyst outlet, so these temperature rises are a result of convection from the upstream reaction.

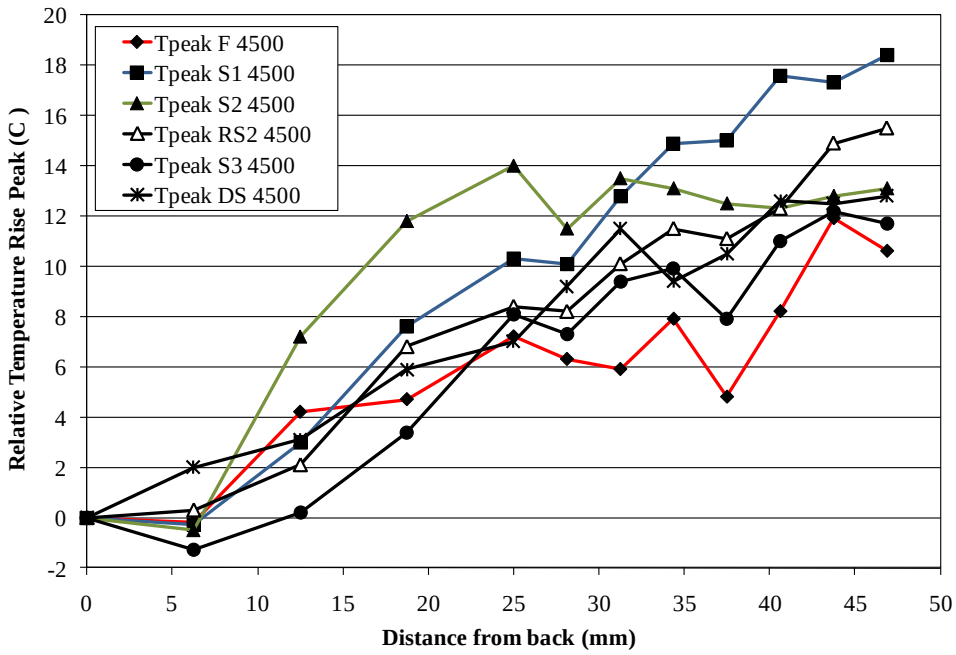

Figure 17. Relative temperature rise peak values as a function of position from the catalyst outlet, with the gas composed of 4500 ppm propylene, 6.5% O_2, 4% H_2O, 300 ppm He, and a balance of N_2.

The completely sulphated S3 catalyst exhibits a profile very similar to the fresh catalyst because these conditions create a more homogeneous catalyst surface for reaction compared to the spatial/localized damage for the S1, S1, and RS2 tests. Close examination suggests that more extensive oxidation occurs toward the catalyst outlet for the fresh catalyst, while the fully-sulphated catalyst is oxidizing more propylene towards the inlet (31.25-50 mm). This observation is attributed to the damaged catalyst only oxidizing small amounts of propylene at the outlet before the reaction zone is shifted forward for back-to-front ignition, such that only the minimum required heat to drive ignition is generated via the exotherm. Further, the inlet temperature is higher for the sulphated catalyst, as the onset of light-off requires a higher temperature as described above. This was also reflected in the concentration light-off profile, where the outlet conversion increases more slowly for the sulphated catalyst (not shown). The desulphated catalyst (DS, desulphated to approximately 38 mm from the outlet) also shows a profile similar to the fresh catalyst in the downstream region, while upstream of 25 mm higher relative temperature rises were observed relative to those of the fresh and fully sulphated catalyst. Higher temperature rises in the inlet relative to downstream would be expected because this portion is less poisoned and so capable of oxidizing more propylene. On the whole, these observations are similar to the temperature rise peak profiles obtained after heterogeneous thermal damage, however the effect of sulphur exposure is more difficult to discern, possibly because the catalyst retains more activity when sulphated (given sufficient temperature) compared to when thermally damaged under the conditions of the previous study.

5.2 Steady-State Inlet Temperature Experiments

The fresh catalyst TPO conversion profile was used to select representative temperatures to study trends when the inlet temperature was held constant; where possible, these same temperatures were used in the subsequent experiment sets to facilitate comparison. While constant inlet temperature is used for the study, the oxidation reactions themselves are not steady-state; however, the term "steady-state" will be used to represent these experiments in contrast to temperature programmed oxidation experiments discussed above. Temperatures were selected from below and above the reaction light-off temperature in addition to the T50. The chosen steady-state experiment inlet temperatures are listed in Table 10 for 4500 ppm C_3H_6. Common temperatures of 180°C and 207°C were also tested to increase the number of comparisons.

Table 10. Steady-state oxidation test temperatures for 4500 ppm propylene.

	F Catalyst	S1 Catalyst	S2/RS2/DS Catalyst	S3 Catalyst
Below light-off	145°C	155°C	165°C	180°C
50% Conversion	155°C	165°C	180°C	207°C
Above light-off	233°C	233°C	233°C	233°C
Common	180°C 207°C	180°C 207°C	207°C	-

The effect of sulphation on steady-state oxidation was less noticeable at the high propylene concentration, compared to activity changes due to heterogeneous thermal aging, because there was still sufficient activity in downstream portions of the catalyst to generate heat and drive ignition at the outlet when the steady-state temperature exceeds the light-off temperature, i.e. the sulphur exposures used here were less

significant in terms of catalyst damage than the thermal aging protocols used previously. Once steady state was achieved after light-off, there was very little difference in the reaction zone profiles at the high propylene concentration, with all temperatures and catalyst conditions obtaining complete conversion within the first 4 mm of catalyst. As such, the reaction zone profiles for the 4500 ppm propylene tests are not shown.

Other spatial metrics demonstrate that the catalyst oxidation performance does change. Table 11 summarizes the light-off position in the catalyst by steady-state inlet temperature and catalyst condition. The method used to determine light-off position is the same described above for heterogeneous thermal deactivation. As explained in Chapter 4 in connection with a sample IRT light-off plot in Figure 18, these values were obtained from the IRT data, and data were collected with a measurement resolution of ~6.25 mm. Similar to the TPO, back-to-front ignition occurs when the temperature exceeds that required for light-off, although it may not occur at the outlet, and as the reaction moves through the catalyst the temperature rise value peaks, followed by a drop when the reaction zone moves further upstream. In this figure, the 37.5 mm position curve rises ahead of those downstream (i.e. 43.75 and 50 mm) and reaches its peak temperature rise before those of upstream positions; the reported light-off position would thus be 37.5 mm. The measurements very clearly show the change in light-off behaviour that occurs, particularly for the 4500 ppm concentration.

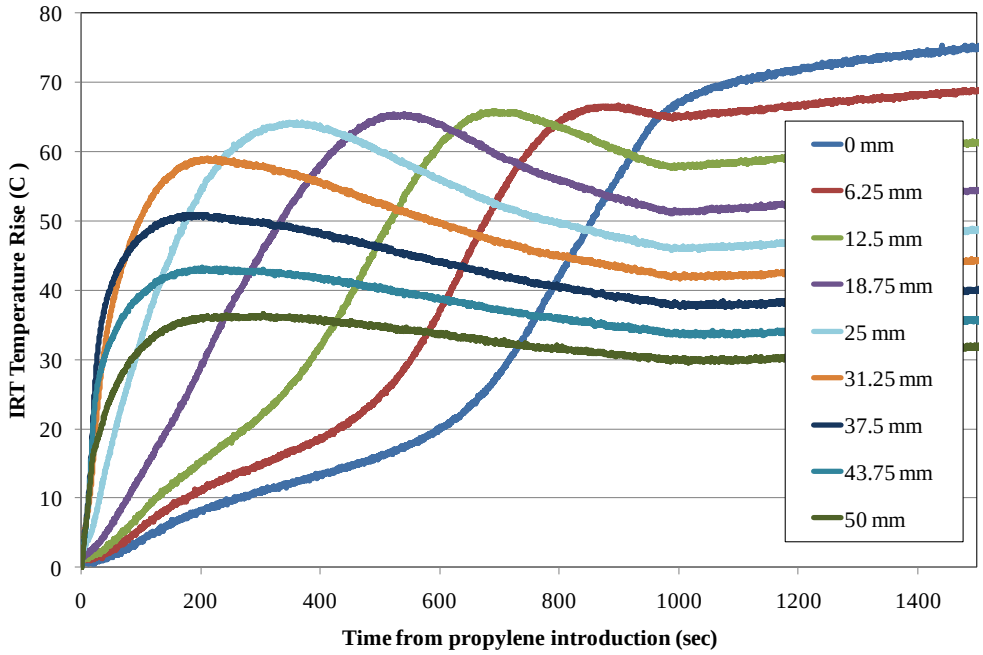

Figure 18. IRT temperature rise light-off sample.Inlet temperature was 180°C with 4500 ppm propylene, 6.5% O_2 and balance N_2 as the inlet gas composition, and the catalyst condition S2.

Table 11. Light-off positions during steady-state experiments with 4500 ppm propylene on sulphur poisoned catalyst.

	Light-off Position (mm from inlet)					
Steady-State Temperature (°C)	F	S1	S2	RS2	S3	DS
165	31.25 *	50	50	25	not tested	none
180	12.5	31.25	37.5	31.25 **	none	50 ***
207	0	25	31.25	7	31.25	25
233	0	12.5	25	0	not tested	0

*155°C was used for the fresh catalyst because 165°C was not tested
**light-off did not start until ~270 seconds after propylene was introduced
***light-off did not start until ~1240 seconds after propylene was introduced

The light-off position moved downstream from that obtained with the fresh catalyst (F) position as the catalyst was progressively sulphated, just as progressive thermal treatment shifted the light-off position downstream. As previously discussed, this light-off position delay occurs because it takes longer for the catalyst to accumulate heat at the back via convection, and some conduction, from the lower levels of reaction exotherm in upstream positions; the addition of sulphur to the catalyst increases the amount of input heat versus generated heat required for the same oxidation performance. The important role of heat transfer for back-to-front ignition has been discussed in Chapter 4, with the build-up of heat from upstream exothermic reactions driving light-off. This was also discussed above, with the TPO data, where the smaller amount of heat generation at the inlet after aging delayed the ignition at the back. A similar effect occurs with the steady-state temperature experiments, however the inlet temperature may exceed that required to generate light-off, so the ignition can occur upstream of the outlet position. The damaged inlet is not able to generate the heat required to ultimately covert all the propylene, and less active sites are available, so more of the catalyst is used which moves the light-off position downstream.

When flipped so the sulphated portion was at the catalyst outlet, some recovery toward the inlet was seen in the measurements of Table 11, because at sufficiently high temperatures the inlet portion of the catalyst plays the most important part in catalyst activity, as discussed in the Chapter 2.3. The third sulphation step (S3) caused another performance decrease. However, the impact of sulphation diminished somewhat at higher temperatures, as noted by the same light-off position at 207°C for catalyst conditions S2 and S3. Because the steady-state inlet temperature was sufficient with the remaining inlet activity to light-off the reaction at 31.25 mm over S2, further sulphation may have shifted the light-off downstream slightly, as a longer light-off time was seen

(described below), but did not shift it far enough to move the light-off to 37.5 mm (ie. the position measurement resolution was insufficient to see the effect of S3 sulphation at 207°C). A similar pattern was seen during TPO, where the back-to-front ignition time (Table 3) was shorter for the more sulphated S2 catalyst than the S1 catalyst during oxidation of 1500 ppm C_3H_6 because the light-off of S1 occurs at a lower temperature. Like the reversed catalyst (RS2), the final step of partial desulphation (DS) resulted in improved oxidation activity (light-off closer to the inlet) relative to most of the sulfated stages, since some sulphur was removed from the catalyst inlet portion; evidence of this sulphur removal from the inlet will be discussed further below with the 1500 ppm propylene data.

To further examine the effect of light-off changes, the MS capillary was located at the same position (7 mm) for every steady-state experiment, until steady-state outlet conversion was attained, after which the capillary was moved to resolve the reaction zone. This allowed for direct comparison of the time required for light-off, as measured by the MS, between the catalyst conditions. Figure 19 shows the conversion light-off profiles for the 180°C steady-state temperature. On the fresh catalyst, there is a fast rise in conversion at 7 mm when propylene is first introduced, indicating that the light-off is very fast. The profile is also very sharp. Conditions S1 and S2 show progressively longer times are required for the catalyst to generate the necessary amount of heat to drive the reaction to the inlet portion, and the broad curving nature of the profiles indicates that the light-off is more gradual, consistent with the TPO data presented above. These results corroborate the shifted light-off position measurement, as when light-off occurred closer to 7 mm, the MS conversion profile is sharper and proceeds from 0 to 100% faster. When the sample was reversed (RS2) and desulphated (DS), the profiles are much sharper, more like the fresh catalyst, because there is a high degree of

activity at the recording position, so the conversion increased rapidly. The fully sulphated catalyst (S3) was unable to achieve light-off at 180°C, obtaining a maximum conversion of less than 10% at 7 mm. Comparisons at 207°C and 233°C depict similar behaviour (not shown).

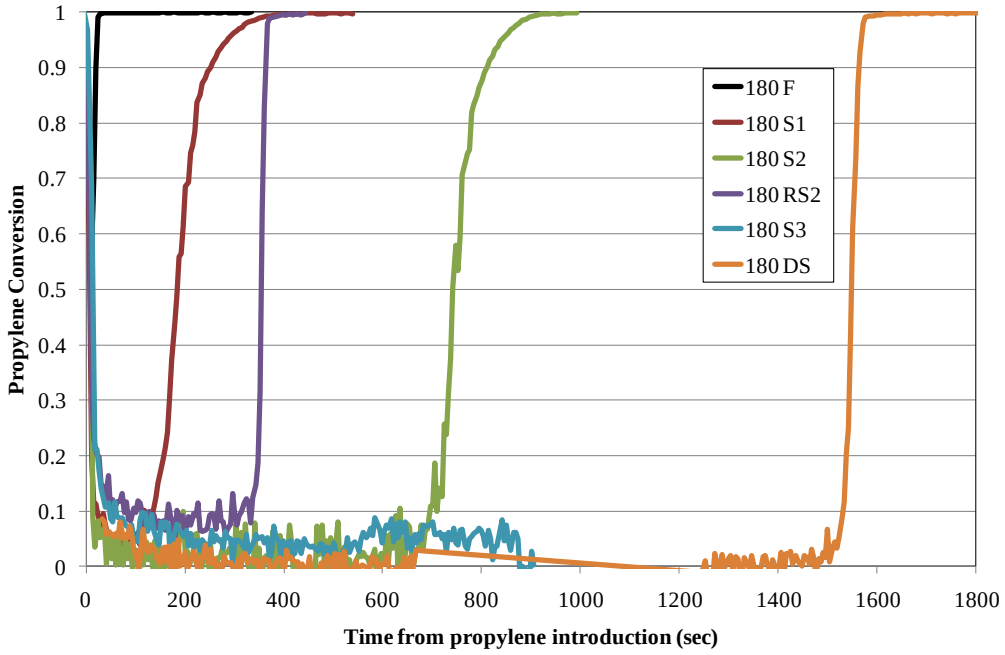

Figure 19. Time for conversion to reach 7 mm from the inlet during steady-state oxidation at 180°C. The gas was composed of 4500 ppm propylene, 6.5% O_2, 4% H_2O, 300 ppm He, and a balance of N_2.

Damage from sulphur was much more apparent in the reaction zone profiles at the lower propylene concentration, compared to the 4500 ppm C_3H_6 tests which showed little difference in reaction zone location once light-off proceeded to the inlet. With 1500 ppm propylene, five temperatures (127°C, 133°C, 145°C, 170°C, and 225°C) were used for comparison. As in the heterogeneous thermal aging discussed in Chapter 4, at the low propylene concentration "stagnant" steady-state reaction zones (no back-

to-front ignition) formed at different locations in the catalyst for each temperature, as seen in Figure 20 and Figure 21, suggesting that heat generation and removal primarily by convection were balanced at this concentration[86,87]. This is in contrast to the 4500 ppm propylene experiments, where at the low temperatures the ignition would also start at the back, but continue to propagate to the inlet, similar to the TPO. This stagnant behaviour can be seen in Figure 20 for the fresh catalyst, where the lowest steady-state inlet temperature (127°C for the fresh sample) did not obtain full conversion (no light-off) in the catalyst length despite the conversion increasing through the length of the catalyst, while at 133°C the reaction zone is located just upstream of the catalyst midpoint but did not advance toward to the inlet with time. It was also noted that full conversion of 1500 ppm was achieved at a lower temperature (133°C) over the fresh (F) catalyst than for 4500 ppm (155°C), which is an effect of less propylene poisoning due to the lower concentration[58]. Exposing the sample to sulphur resulted in the reaction zone location shifting downstream, which can be seen most clearly by comparing the 145°C reaction zones of Figure 20 and 170°C zones of Figure 21. Interestingly, the incomplete conversion at 145°C for condition RS2 shows that after the midpoint of the catalyst the activity levels off. With the sulphated portion of catalyst located at the outlet, there is no significant amount of reaction occurring, in contrast to samples with sulphur at the inlet (127°C F, 133°C S1 and S2, 145°C S2), which show conversion increases, albeit small, through the entire catalyst length. Further, there is a drop in the outlet conversion noted between S1 and S2 at 133°C, due to increased catalyst damage. This same pattern was seen for the other catalyst conditions at temperatures below light-off (not shown).

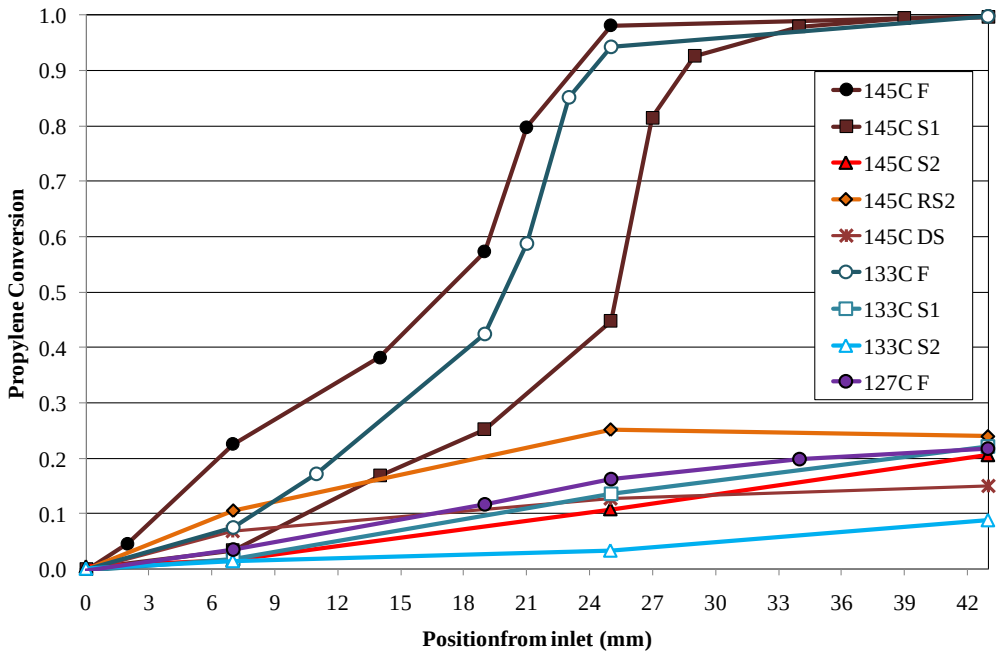

Figure 20. Low temperature steady-state, spatially-resolved conversion profiles over the first 43 mm of catalyst (last point measured).The gas composition was 1500 ppm propylene, 6.5% O_2, 4% H_2O, 300 ppm He, and a balance of N_2.

The reaction zones for the high temperature steady-state tests are shown in Figure 21. At the highest inlet temperature (225°C), the reaction zone was very close to the catalyst inlet. For brevity, only the fresh and fully sulphated catalyst reaction zones at 225°C are shown, but these zones are essentially the same. At 170°C, there is also a marked increase in the width of the reaction zone following sulphation as more catalyst volume is required to achieve the same conversion performance. Both a shift downstream and an increase in width of the reaction zones were also noted following thermal aging at 1500 ppm. For the fresh and RS2 catalyst, the reaction zone is contained between 0 and 4 mm from the inlet. Following the first sulphation, the reaction zone covered 0 to 11 mm, and the S2 catalyst extended it from 7 to 29 mm. Full sulphation of the catalyst did not permit light-off of the reaction at this temperature

because insufficient heat was generated in upstream portions, an effect also seen for the 4500 ppm C_3H_6 tests as indicated in Table 11.

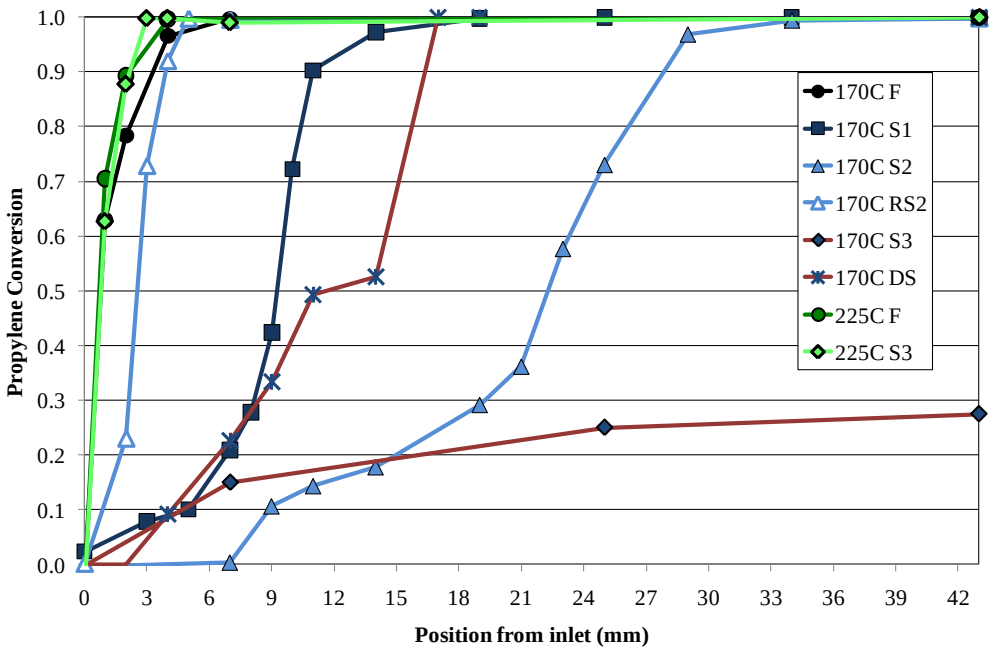

Figure 21. Steady-state, spatially-resolved conversion profiles over the first 43 mm of catalyst (last point measured). The gas composition was 1500 ppm propylene, 6.5% O_2, 4% H_2O, 300 ppm He, and a balance of N_2.

The results for RS2 show that after the catalyst was rotated, activity in the inlet portion was regained, in particular for 170°C. At that temperature, following S1, the reaction zone had moved from the very inlet to around 9 mm and to half the catalyst length following S2, while the reaction zone for RS2 is located between 2-5 mm. Following desulphation there was movement of the 170°C reaction zone profile forward to slightly downstream of the S1 profile, while lying approximately 10 mm in front of the S2 profile, which is also reflected in the light-off position measurements. These observations are also reflected in the light-off location measurements for 1500 ppm

propylene, listed in Table 12. Again, no change in the light-off location was measured for 225°C.

Table 12. Light-off positions during steady-state experiments with 1500 ppm propylene on sulphur poisoned catalyst.

	Light-off Position (mm from inlet)					
Steady-State Temperature (°C)	F	S1	S2	RS2	S3	DS
145	18.75	37.5	none	none	-	none
170	0	18.75	37.5	12.5	None	12.5
225	0	0	0	0	0	0

Chapter 6: Conclusions

The effect of heterogeneous damage was assessed by studying the changes that occurred during propylene oxidation over a model Pt/Al_2O_3 diesel oxidation catalyst. Heterogeneous thermal damage was accomplished by pulsing propylene and oxygen into the reactor at 500°C, resulting in the inlet section of catalyst experiencing temperatures above 650°C to induce Pt sintering. Dispersion measurements suggest that the catalyst aged for 1 hour at 790°C (the hottest temperature measured during aging) has approximately 25% of the Pt dispersion measured on the fresh catalyst. Heterogeneous sulphur damage was attained by feeding SO_2 with oxygen to the reactor at 375°C until breakthrough was seen with the SpaciMS at different inlet positions in the catalyst. Actual measurement of the catalyst sulphur content was not possible without catalyst destruction, however sulphur is assumed to deposit more heavily in upstream positions. A partially desulphated catalyst, achieved by H_2 reduction at 400°C and measured by sulphur desorption from the catalyst, was also compared to the sulphated catalyst states. Infrared thermography and SpaciMS techniques were used to characterize spatial temperature and concentration profiles before and after the damage processes.

Thermal degradation of the catalyst inlet increased the temperature for light-off (T50) during temperature programmed oxidation. As well, the temperature and conversion waves traveled more slowly in back-to-front ignition; the time between successive temperature peaks also increased, particularly in the inlet portion of the catalyst that

was more damaged. The peak temperature rise values decreased in the inlet portion of the catalyst following aging as less propylene was reacting at these positions.

During steady-state oxidation tests, thermal aging moved the reaction zone downstream from the inlet, except at very high temperatures (233°C) where the reaction zone was consistently within the first few millimetres of catalyst. At low temperatures with 4500 ppm C_3H_6, when reaction light-off occurred, back-to-front ignition was consistently observed on fresh and aged catalysts. When the lower concentration of 1500 ppm was introduced at low temperatures, light-off could still occur, but the reaction zone was formed at a location within the catalyst and did not propagate forward due to the smaller amount of heat generated. When aged, the reaction zones for 1500 ppm C_3H_6 experienced a discernible movement downstream and an increase in width. For both concentrations, aging shifted the light-off position measured by IRT downstream. The movement of the reaction zones occurs because the damaged catalyst oxidizes less propylene in the inlet of the catalyst, so more of the catalyst is required to achieve the same outlet performance.

Similar to the thermal deactivation, catalyst sulphation of the inlet increased the light-off temperature (T50), as well as the time for the temperature and conversion waves to travel from the back-to-front during TPO experiments. When the sample was reversed to position the sulphated zone at the outlet, and when fully sulphated, the time from the reference temperature to the light-off increased, while the time for back-to-front ignition decreased substantially. This was consistent with the different slope patterns of the peak time versus location curves.

Likewise, the behaviour of 1500 ppm propylene during steady-state experiments showed the same stagnant reaction zone behaviour as the thermally-aged catalyst following light-off, with a movement of the zone downstream following sulphation. Unlike with thermal damage, when 4500 ppm propylene was oxidized the steady-state reaction zones established following back-to-front ignition were all very similar. However, the IRT steady-state oxidation profiles measured a change in the light-off locations that illustrate activity changes for both the high and low concentrations, specifically a movement of the light-off location downstream following sulphur addition steps, and a movement upstream following a step to remove sulphur from the inlet (simulated and real desulphation). This reflects the observation that the extent of sulphur damage was less severe for catalyst activity than thermal aging, with the catalyst retaining good activity given sufficient temperature. Following removal of some sulphur from the inlet portion of the catalyst by desulphation, oxidation performance improved from the fully sulphated (S3) state at all temperatures and for both propylene concentrations.

Overall, the spatial temperature and concentration changes that occurred with heterogeneous catalyst damage were similar in nature. However, the extent of damage created by sulphation, and thus the degree of change to the spatial profiles, were less prominent than those observed with thermal aging. The likely cause is that while sulphur damage can diminish the oxidation capacity of the catalyst, given sufficient temperature the overall performance can be retained, while the thermally damaged catalyst is unable to do this because of major structural changes associated with thermal sintering. As well, it is noted that while at least some of the catalyst activity can be recovered with a desulphation process, there is currently no in-situ method to redisperse sintered precious metal.

Chapter 7: Recommendations

1) The experiments should be repeated with other commonly studied reactants, such as CO, NO, and different hydrocarbons (e.g. alkanes and higher-order hydrocarbons), to determine how each of these is affected by heterogeneous catalyst damage. This might indicate whether the damage is occurring to the Pt metal more than the washcoat, information that is pertinent to catalyst design.
2) The experiments should be repeated with more complicated reactant mixtures that more closely approximate diesel engine exhaust, to verify that the same patterns are observed.
3) Investigate in-situ and non-destructive methods to study the state/properties of the catalyst. This information would be invaluable for future modeling of the heterogeneous catalyst damage and how it affects overall catalyst performance.
4) Study heterogeneous aging over zone-coated/non-uniform distribution catalysts to determine how the non-uniform properties react to the heterogeneous damage.
5) Investigate a controllable furnace for the camera reactor that will improve the ability to tune the temperature of the reactor and increase the precision for steady-state temperatures despite changes in the lab environment and operator.

References

[1] S.R. Katare, J. E. Patterson, and P. M. Laing. Ind. Eng. Chem. Res. 46 (2007) 2445.
[2] G. Corro. React. Kinet. Catal. Lett. 75(2002) 89.
[3] T.V. Johnson. Int. J. Eng. Res. 10 (2009) SI 275.
[4] F. Haaß and H. Fuess. Adv. Eng. Mat. 7 (2005) 899.
[5] W.A. Majewski, M.K. Khair. Diesel Emissions and Their Control. Warrendale, PA: SAE International. 2006.
[6] R.P.Wayne, Chemistry of Atmospheres: An Introduction to the Chemistry of the Atmospheres of Earth the Plants and their Satellites, third ed., Oxford University Press, 2000.
[7] Heck R, Farrauto RJ. Catalytic Air Pollution Control. New York: Van Nostrand Reinhold; 1995
[8] Robert J. Farrauto. React. Kinet. Catal. Lett. 60 (1997) 233.
[9]. K.F. Hansen, F. Bak, M. Andersen, H. Bejder, H. Autrup. SAE Technical Paper Series 940241 (1994).
[10] D.E. Webster, Top. Catal. 16/17 (2001) 33.
[11] Clean Air Act. United States Environmental Protection Agency (2008). Retrieved August 23, 2010: http://www.gpo.gov/fdsys/pkg/USCODE-2008-title42/pdf/USCODE-2008-title42-chap85.pdf.
[12] Euro 5 and Euro 6 standards: reduction of pollutant emissions from light vehicles. Europa – Summaries of EU Legislation. Jan. 7, 2010. Retrieved July 14, 2010: http://europa.eu/legislation_summaries/environment/air_pollution/l28186_en.htm
[13] M.V. Twigg. Catal. Today 117 (2006) 407.
[14] Y. Yao, J. Catal. 46 (1977) 388.
[15] S. Katare, P. Laing. SAE Technical Paper Series 2006-01-0689 (2006).
[16] E. Xue, K. Seshan, J.R.H. Ross. Appl. Catal. B: Environ. l 11 (1996) 65.
[17] N. Takahashi, H. Shinjoh, T. Iijima, T. Suzuki, K. Yamazaki, K. Yokota, H. Suzuki, N. Miyoshi, S. Matsumoto, T. Tanizawa, T. Tanaka, S. Tateishi, K. Kasahara. Catal. Today 27 (1996) 63.
[18] S. Hodjati, P. Bernhardt, C. Petit, V. Pitchon, A. Kiennemann. Appl. Catal. B: Environ. 19 (1998) 209.
[19] S. Erkfeldt, E. Jobson, M. Larsson. Top. Catal. 16/17 (2001) 127.
[20] L. Olsson, H. Persson, E. Fridell, M. Skoglundh, B. Andersson, J. Phys. Chem. B 105 (2001) 6895.
[21] A. Kato, S. Matsuda, T. Kamo, F. Nakajima, H. Kuroda and T. Narita, J. Phys. Chem. 85 (1981) 4099.
[22] S.R. Katare, J.E. Patterson and P.M. Laing. SAE Technical Paper Series 2007-01-3984 (2007).
[23] C. Yokoyama and M. Misono. J. Catal. 150 (1994) 9.
[24] R. Burch, J.A. Sullivan, T.C. Watling. Catal. Today 42 (1998) 13.
[25] M. Koebel, G. Madia, M. Elsener. Catal. Today 73 (2002) 239.
[26] L. Olsson and E. Fridell. J. Catal. 210 (2002) 340.
[27] J. Després, M. Elsener, M. Koebel, O. Kröcher, B. Schnyder, A. Wokaun. Appl. Catal. B: Environ. 50 (2004) 73.

[28] M. Kaneeda, H. Iizuka, T. Hiratsuka, N. Shinotsuka, M. Arai. Appl. Catal. B: Environ. 90 (2009) 564.
[29] L. Olsson, H. Karlsson. Catal. Today 147S (2009) S290.
[30] S. Hodjati, K. Vaezzadeh, C. Petit, V. Pitchon, A. Kiennemann. Catal. Today 59 (2000) 323.
[31] W.S. Epling, L.E. Campbell, A. Yezerets, N. W. Currier; J.E. Parks II. Catal. Rev. 46 (2004) 163.
[32] A. Setiabudi, M. Makkee, J.A. Moulijn, Appl. Catal. B: Environ. 50 (2004) 185.
[33] J. Jung, S. Song, K. Min Chun. SAE Technical Paper Series 2008-01-0482 (2008).
[34] D.D. Beck , J.W. Sommers, C.L. DiMaggio. Appl. Catal. B: Environ. 11 (1997) 257.
[35] C.P. Hubbard, K. Otto, H.S. Gandhi, K.Y.S. Ng, J. Catal. 139 (1993) 268.
[36] A.K. Neyestanaki, F. Klingstedt, T. Salmi, D.Yu. Murzin. Fuel 83 (2004) 395.
[37] J. Andersson, M. Antonsson, L. Eurenius, E. Olsson, M. Skoglundh. Appl. Catal. B: Environ. 72 (2007) 71.
[38] S.T. Oh, S.M. Kim, M.S. Yoon, H.K. Lee, G.K. Yeo, H.I. Lee. React. Kinet. Catal. Lett. 90 (2007) 339.
[39] A. Winkler, D. Ferri, M. Aguirre. Appl. Catal. B:Environ. 93 (2009) 177.
[40] L.O. Lowendahl and J.-E. Otterstedt, Appl. Catal. 59 (1990) 89.
[41] M. Skoglundh, L.O. Lawendahl and J.-E. Ottersted. App. Catal., 77 (1991) 9.
[42] J.T. Kummer, Prog. Energy Cornbust. Sci., 6 (1980) 177.
[43] A. Ishikawa, S. Komai, A. Satsuma, T. Hattori, Y. Murakami. Appl. Catal. A: Gen. 110 (1994) 61.
[44] H. Yoshida, Y. Yazawa, N. Takagi, A. Satsuma, T. Tanaka, S. Yoshida, and T. Hattori. J. Synchrotron Rad. 6 (1999) 471.
[45] R. M. Heck, R. J. Farrauto. Appl. Catal. A: Gen. 221 (2001) 443.
[46] M.J. Patterson, D.E. Angove, N.W. Cant. Appl. Catal. B: Environ. 26 (2000) 47.
[47] T. Mang, B. Breitscheidel, P. Polanek, H. Knozinger, Appl. Catal. A: Gen. 106 (1993) 239.
[48] M.K. Oudenhuijzen, P.J. Kooyman, B. Tappel, J.A. van Bokhoven, D.C. Koningsberger, J. Catal. 205 (2002) 135.
[49] K. Hauff, U. Tuttlies, G. Eigenberger, U. Nieken.
App. Catal. B, Environ. (2010), published online - doi:10.1016/j.apcatb.2010.07.036
[50] J. Segner, W. Vielhaber, G. Ertl, Isr. J. Chem. 22 (1982) 375.
[51] J. Volter, G. Lietz, H. Spindler, H. Lieske, J. Catal. 104 (1987) 375.
[52] E.S. Putna, J.M. Vohs, R.J. Gorte. Surf. Sci. 391 (1997) L1178.
[53] V.P. Ivanov, V.I. Savchenko, G.K. Boreskov, K.C. Taylor. Kinet. Catal. 19 (1978) 163.
[54] A. Barresi, G. Baldi, Chem. Eng. Sci. 47 (1992) 1943.
[55] S. Ordóñez, L. Bello, H. Sastre, R. Rosal, F.V. Diez. Appl. Catal. B: Environ. 38 (2002) 139.
[56] Y.-F. Yu Yao, Ind. Eng. Chem. Prod. Res. Dev. 19 (1980) 293.
[57] M. Sheintuch, D. Luss. J. Catal. 68 (1981) 245.
[58] S.E. Voltz, C.R. Morgan, D. Liederman, S.M. Jacob. Ind. Eng. Chem. Prod. Res. Develop. 12 (1973) 294.
[59] J.W.A. Schlangen, G.W. Neuhaus, M. Madani, W.F. Maier, J. Prakt. Chem. 334 (1992) 465.
[60] T. Watanabe, K. Kawashima, Y. Tagawa, K. Tashiro, H. Anoda, K. Ichioka, S. Sumiya, G. Zhang. SAE Technical Paper Series 2007-01-1920 (2007).
[61] J.J. Spivey, Ind. Eng. Chem. Res. 26 (1987) 2165.
[62] A.A. Barresi, G. Baldi, Ind. Eng. Chem. Res. 33 (1994) 2964.

[63] K. Irani, W.S. Epling, R. Blint. Appl. Catal. B: Environ. 92 (2009) 422.
[64] W.I. Patterson, C. Kemball. J. Cal. 2 (1963) 465.
[65] A. Schwartz, L.L. Holbrook, H. Wise, J. Catal., 21 (1971) 199.
[66] N.W. Cant, W.K. Hall, J. Catal. 16 (1970) 220.
[67] L.M. Carballo, E.E. Wolf. J. Catal. 53 (1978) 366.
[68] E. McCarthy, J. Zahradnik, G.C. Kuczynski, J.J. Carberry. J. Catal. 39 (1975) 29.
[69] E. Ruckenstein, M.L. Malhotra. .J. Catal. 41 (1976) 303.
[70] R.M.J. Fiedorow, S.E. Wanke. J. Catal. 43 (1976) 34.
[71] E.I. Altman, R.J. Gorte. Surf. Sci. 172 (1986) 71.
[72] E.I. Altman, R.J. Gorte. Surf. Sci. 195 (1988) 392.
[73] P. Pareja, A. Amariglo, G. Piquard, H. Amariglio. J. Catal. 46 (1977) 225.
[74] Y. Morooka, A. Ozaki. J. Catal. 5 (1966) 116.
[75] O. Shakir, A. Yezerets, N. Currier, W.S. Epling. Appl. Catal. A: Gen. 365 (2009) 301.
[76] D. Luss. Ind. Eng. Chem. Res. 36 (1997) 2931.
[77] M. Sheintuch, I. Keren. Chem. Eng. Sci. 55 (2000) 1461.
[78] D. Luss, M. Sheintuch. Catal. Today 105 (2005) 254.
[79] K. Chen, K.S. Martirosyan, D. Luss. Ind. Eng. Chem. Res. 48 (2009) 8451.
[80] S.H. Oh, J.C. Cavendish, AIChE Journal 35 (1985) 935.
[81] D. Schmitt, H. Fuess, H. Klein, U. Neuhausen, E.S. Lox. Top. Catal 16/17 (2001) 355.
[82] A. Winkler, D. Ferri, M. Aguirre. Appl. Catal. B: Environ. 93 (2009) 177.
[83] F.M.Z. Zotin, O.F.M. Gomes, C.H. de Oliveira, A.A. Neto, M.J.B. Cardoso. Appl. Catal. A: Gen. 107/108 (2005) 157.
[84] D.D. Beck, J.W. Sommers, C.L. DiMaggio. App. Cat. A: Gen. 11 (1996) 257.
[85] C.K. Lambert, Y. Cheng, D. Dobson, J. Hangas, M. Jagner, H. Jen, J. Warner. SAE Technical Paper Series 2009-01-2711 (2009).
[86] S. Tronci, R. Baratti, A. Gavriilidis. Chem. Eng. Comm. 173 (1999) 53.
[87] V. Cominos, A. Gavriilidis. Chem. Eng. Sci. 56 (2001) 3455.
[88] N.R. Collins, J.A. Cooper, D. Morris, A. Ravenscroft, M.V. Twigg. SAE Technical Paper Series 2005-01-2158 (2005).
[89] Y.D. Kim, S.J. Jeong, W.S. Kim. Chem. Eng. Sci. 64 (2009) 1373.
[90] H.S. Gandhi, M. Shelef. Appl. Catal. 77 (1991) 175.
[91] J. Guthrie. Sulphur in Liquid Fuels 2006. Environment Canada. 2008. Retrieved March 4, 2010: http://www.ec.gc.ca/cleanair-airpur/5B4D506F-E73E-440A-B9CE-7C805D4FD15D/Sulphur_in_Liquid_Fuels_2006-En.pdf
[92] D.L. Mowery, R.L. McCormick. Appl. Catal. B: Environ. 34 (2001) 287.
[93] Y. Takahashi, Y. Takeda, N. Kondo, M. Murata. SAE Technical Paper Serie 2004-01-0580 (2004).
[94] K. Yoshida, T. Asanuma, H. Nishioka, K. Hayashi, S. Hirota. SAE Technical Paper Series 2007-01-0237 (2007).
[95] E. Xue, K. Seshan, J.G. van Ommen, J.R.H. Ross. Appl. Catal. B: Environ. 2 (1993) 183.
[96] A. Hinz, M. Skoglundh, E. Fridell, A. Amberntsson, J. Catal. 201 (2001) 247.
[97] K.C. Taylor. Ind. Eng. Chem., Prod. Res. Dev. 15 (1976) 264.
[98] P. Zelenka, W. Cartellieri, P. Herzog. Appl. Catal. B: Environ. 10 (1996) 3.
[99] C.C. Chang. J. Catal. 53 (1978) 374.
[100] H.C. Yao, H.K. Stepien, H.S. Gandhi. J. Catal. 67 (1981) 231.
[101] A. Datta, R.G. Cavell, R.W. Tower, Z.M. George. J. Phys. Chem. 89 (1985) 443.
[102] O. Saur, M. Bensitel, A.B.M. Saad, J.C. Lavalley, C.P. Tripp, B.A. Morrow. J. Catal. 99 (1986) 104.

[103] R. Burch, E. Halpin, M. Hayes, K. Ruth, J.A. Sullivan. Appl. Catal. B: Environ. 19 (1998) 199.
[104] N.M. Popova, A.K. Umbetkaliev, K. Dosumov, N.A. Antonova, React. Kinet. Catal. Lett. 57 (1996) 255.
[105] F. Cabello Galisteo, C. Larese, R. Mariscal, M. Lopez Granados, J.L.G. Fierro, R. Fernandez-Ruiz, M. Furio. Top. Catal. 28 (2004) 451.
[106] F. Cabello Galisteo, R. Mariscal, M. Lopez Granados, J.L.G. Fierro, P. Brettes, O. Salas. Environ. Sci. Technol. 39 (2005) 3844.
[107] J.A. Lampert, M.S. Kazi, R.J. Farrauto, Appl. Catal. B: Environ.14 (1997) 211.
[108] D.L. Mowery, R.L. McCormick. Appl. Catal. B: Environ. 34 (2001) 287.
[109] J.-R. Chang, S.-L. Chang, T.-B. Lin. J Catal. 169 (1997) 338.
[110] Z. Paal, K. Matusek, M. Muhler. Appl. Catal. A: Gen. 149 (1997) 113.
[111] A.F. Lee, K. Wilson, R.M. Lambert, C.P. Hubbard, R.G. Hurley, H.S. Gandhi. J. Catal. 184 (1999) 491.
[112] J.A. Rodriguez, J. Hrbek. Acc. Chem. Res. 32 (1999) 719.
[113] G. Corro, J.L.G. Fierro, V.C. Odilon. Catal. Comm. 4 (2003) 371.
[114] F. Cabello Galisteo, R. Mariscal, M. Lopez Granados, M.D. Zafra Poves, J.L.G. Fierro, V. Kroger , R.L. Keiski. App. Catal. B: Environ. 72 (2007) 272.
[115] R. Burch, T.C. Watling. App. Catal. B: Environ. 17 (1998) 131.
[116] M. Skoglundh, A. Ljungqvist, M. Petersson, E. Fridell, N. Cruise, O. Augustsson, E. Jobson. Appl. Catal. B: Environ. 30 (2001) 315.
[117] T.-C. Yu, H. Shaw. Appl. Catal. B: Environ. 18 (1998) 105.
[118] J. Chen, R.M. Heck, R.J. Farrauto. Catal. Today 11 (1992) 517.
[119] J.M. Jones, V.A. Dupont, R. Brydson, D.J. Fullerton,
N.S. Nasri, A.B. Ross, A.V.K. Westwood. Catal. Today 81 (2003) 589.
[120] J.-Y. Luo, D. Kisinger, A. Abedi, W.S. Epling. Appl. Catal. A: Genl 383 (2010) 182.
[121] D.J. Fullerton, A.V.K. Westwood, R. Brydson, M.V. Twigg, J.M. Jones. Catal. Today 81 (2003) 659.
[122] C.S. Sharma, R. Hughes. Chem. Eng. Sci. 34 (1979) 625.
[123] M. Sun, E.B. Croiset, R.R. Hudgins, P.L. Silveston, M. Menzinger. Ind. Eng. Chem. Res. 42 (2003) 37.
[124] A. Jaree, R.R. Hudgins, H. Budman, P.L. Silveston, V. Yakhnin, M. Menzinger. Chem. Eng. Sci. 58 (2003) 833.
[125] M. Menzinger, V. Yakhnin, A. Jaree, P.L. Silveston, R.R. Hudgins. Chem. Eng. Sci. 59 (2004) 4011.
[126] J.S. Choi, W.P. Partridge, C.S. Daw. Appl. Catal. A: Gen. 293 (2005) 24.
[127] J.S. Choi, W.P. Partridge, W.S. Epling, N.W. Currier, T.M. Yonushonis. Catal. Today. 114 (2006) 102.
[128] J.S. Choi, W.P. Partridge, C.S. Daw, Appl. Catal. B: Environ. 77(2007) 145.
[129] J.S. Choi, W.P. Partridge, J. Pihl, C.S. Daw, Catal. Today 136 (2008) 173.
[130] A. Russell, W.S. Epling, H. Hess, H.-Y. Chen, C. Henry, N. Currier, A. Yezerets. Ind. Eng. Chem. Res. 49 (2010) 10311. DOI: 10.1021/ie1005299.
[131] V. Yakhnin, M. Menzinger. AlChE Journal 44 (1998) 1222.
[132] M.S. Kulkarni, M.P. Dudukovic. Chem. Eng. Sci. 51 (1996) 3083.
[133] A. Jaree, H. Budman, R.R. Hudgins, P.L. Silveston, V. Yakhnin, M. Menzinger. Catal. Today. 69 (2001) 137.

APPENDIX A

Statistical Significance of Measurements

To show that the reaction zone measurement results are statistically significant/reproducible, confidence intervals were calculated. The confidence interval parameter describes the boundaries within which the mean is expected to fall, and this boundary depends on the confidence level. This method assumes that there is no systematic error in the measurement collection system or the experiment. As well, due to the small sample size, the t-distribution was used instead of the normal distribution.

The calculation of the confidence interval is described by Equation 3,

$$\left(CI_{higher}, CI_{lower}\right) = X \pm t_{\alpha/2,n-1} * \frac{S}{\sqrt{n}} \quad (3)$$

where X is the sample mean value, S is the sample standard deviation, and n is the sample size; standard error (SE) can also be used to refer to the last term in the expression.

The reaction zone spatial measurements at steady-state were collected with a measurement resolution of ~ 1 mm. At each measurement position, the MS collected multiple concentration measurements. Experiments were replicated, and the confidence interval parameters calculated with the combined data. A sample of the standard error values is shown in Table A1, calculated from the steady-state oxidation of 1500 ppm propylene at 170°C over the A1 (thermally damaged) catalyst sample. The confidence level of the calculation is 90%.

Table 13. Statistical parameters calculated from steady-state oxidation of 1500 ppm propylene at 170°C on A1 catalyst.

Position from Inlet (mm)	Standard Deviation *S*	Sample Size *n*	Standard Error *SE*	Propylene Conversion	CI_{higher}	CI_{lower}
0	0.048	106	0.005	0.08	0.09	0.07
1	0.058	98	0.006	0.08	0.09	0.07
5	0.060	101	0.006	0.10	0.11	0.08
7	0.061	93	0.006	0.11	0.12	0.10
11	0.063	129	0.006	0.18	0.20	0.17
14	0.159	151	0.013	0.58	0.60	0.55
17	0.052	96	0.005	0.97	0.98	0.96
19	0.070	106	0.007	0.97	0.99	0.96
25	0.066	127	0.006	0.98	1.00	0.97
43	0.078	111	0.007	1.00	1.01	0.98

The standard error values are smaller than the level of sensitivity recorded for the conversion value, which is plotted versus spatial location to create the reaction zone profile. The confidence interval describes where 90% of sample means will contain the true mean value of propylene concentration for each position. A visual representation of the data presented above is shown in Figure A1.

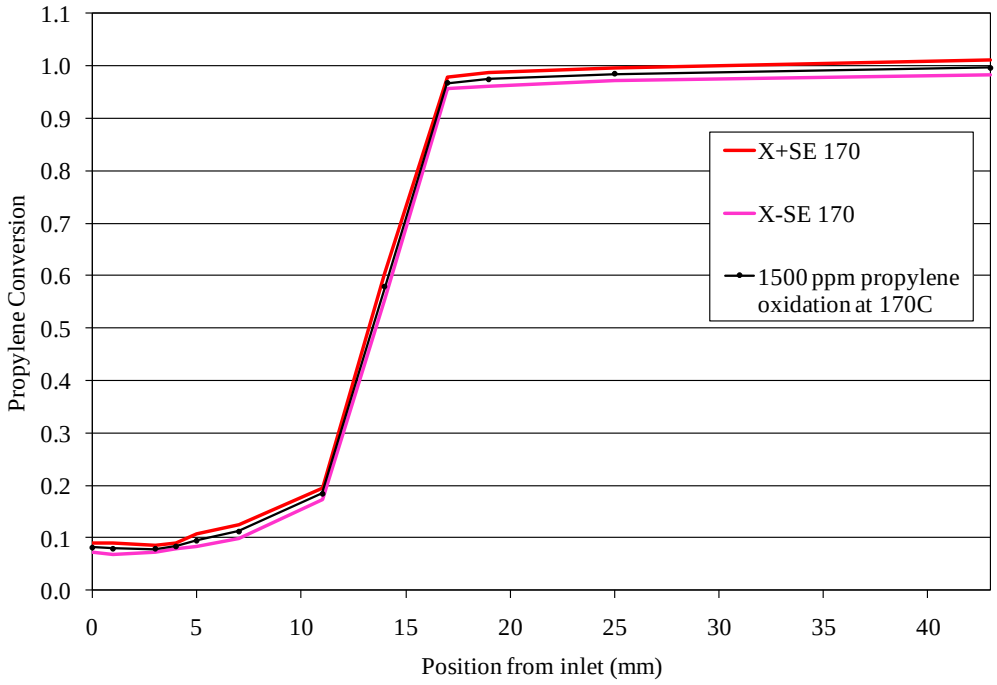

Figure 22. Calculated confidence interval on reaction zone at 170°C. The gas composition was 1500 ppm propylene, 6.5% O_2, 4% H_2O, 300 ppm He, and a balance of N_2.